Geophys. J. Int. (2006) **164,** 516–542 doi: 10.1111/j.1365-246X.2006.02871.x

Characterizing swells in the southern Pacific from seismic and infrasonic noise analyses

Guilhem Barruol,[1,2] Dominique Reymond,[3] Fabrice R. Fontaine,[1] Olivier Hyvernaud,[3] Vincent Maurer[3] and Keitapu Maamaatuaiahutapu[2]

[1] *Laboratoire de Tectonophysique, CNRS, Univ. Montpellier II,* 34095 *Montpellier, France*
[2] *Laboratoire Terre-Océan, Université de Polynésie française,* BP 6570, 98702 *Faaa Aéroport, Tahiti, Polynésie française. E-mail: barruol@upf.pf*
[3] *Laboratoire de Géophysique, Commissariat à l'énergie atomique, Pamatai, Tahiti, Polynésie française*

Accepted 2005 November 4. Received 2005 June 20; in original form 2005 April 20

SUMMARY

A temporary network of 10 broad-band seismic stations has been installed in French Polynesia for the Polynesian Lithosphere and Upper Mantle Experiment (PLUME). All the seismic stations were installed either on volcanic islands or on atolls of the various archipelagos of French Polynesia in a manner which complements the geographic coverage provided by the regional permanent stations. The primary aim of PLUME is to image the upper mantle structures related to plate motion and hotspot activity. However, because of its proximity to all sites, the ocean is responsible for a high level of noise in the seismic data and we show that these data can also be used to analyse ocean wave activity. The power spectral density (PSD) analyses of the seismic data recorded in French Polynesia show clear peaks in the 0.05–0.10 Hz band (periods between 10 and 20 s), which corresponds to swell frequencies. Clear peaks in this frequency band are also observed in infrasonic data recorded on Tahiti. Ground motion analysis shows that the swell-related seismic noise (SRSN) is linearly polarized in the horizontal plane and its amplitude decreases rapidly with the distance from the shore. The microseismic and the infrasonic 'noise' amplitudes show very similar variations from station to station and both are strongly correlated with the swell amplitudes predicted by the National Oceanic and Atmospheric Administration (NOAA), wind-forced, 'WaveWatch' models. The swell direction can be estimated from SRSN polarization analysis but this has to be done with care since, for some cases, the ground motions are strongly controlled by the islands' anisometric shapes and by swell refraction processes. We find cases, however, such as Tahiti or roughly circular Tuamotu atolls, where the azimuth of the swell is in good agreement with the seismic estimates. We, therefore, demonstrate that the SRSN and the infrasonic signal observed in French Polynesia can be used in such cases as a proxy for swell amplitude and azimuth. From the continuous analysis of the data recorded in 2003 at the permanent seismic station PPTL in Tahiti, transfer functions have been obtained. This could provide a way to quantify the swell activity during the last two decades and, therefore, assist in the investigation of climate changes.

Key words: French Polynesia, infrasound, oceanic waves, oceans, polarization, seismic noise, swell.

1 INTRODUCTION

French Polynesia situated in the southern Pacific Ocean, between 10 and 30° South in latitude is generally not affected by deep atmospheric depressions, except during the occasional and short-duration cyclones. This is, therefore, not a region where storm-generated swells often originate. However, the region is affected each year by numerous swell episodes generated by atmospheric depressions, which have developed at higher latitudes, in both the northern and the southern Pacific. The absence of direct measurements of swell height by buoys in this South Pacific area requires the use of other, indirect, ways to characterize swells. Investigating the use of geophysical observables such as seismic and infrasonic data as proxies for ocean wave activity, swell observation and forecasting is, therefore, the primary aim of this paper.

Buoy 51028 is located close to the Christmas Island, on the Equator at a longitude of 153° west. Although this buoy is more than 2000 km from Tahiti island, it is the nearest moored buoy to

French Polynesia so we have examined the monthly statistical analysis of the data from this location (available from the National Data Buoy Center http://seaboard.ndbc.noaa.gov/index.shtml) for the period 1997–2001. The significant wave height *Hs* (i.e. the average height of the highest one-third of the waves) varies between 1.0 and 3.5 m during the year, except in May, June and August when it can be less than 0.5 m. The mean value of the significant wave height for the 5-yr period analysed is 2.0 m with a standard deviation of 0.4 m. The dominant wave period varies between 5 and 20 s, except for the months of May, June and August, when local seas of shorter periods may dominate. The mean swell period over the 5 yr is 11.2 s with a standard deviation of 3.0 s. Swell of period 20 s can occur at any time of the year, except during the month of August. The long period ($>$11 s) swells recorded at the equatorial buoy installed at Christmas Island are not generated by local winds, which should induce waves of higher frequencies. They have instead remote origins, such as the North Pacific storms, which occur during the boreal winters, and the South Pacific atmospheric depressions, which occur during the austral winters. Such swell events generated at high latitudes cross the whole Pacific Ocean, including the French Polynesia region in the South Pacific. The mean value of the swell height and the dominant periods of the swell in French Polynesia are, therefore, not expected to differ greatly from those observed at the equatorial buoy.

The buoy measurements obtained at Christmas Island are in agreement with daily values of swell *Hs* around Tahiti island derived from synoptic maps combining visual observations and satellite data. The latter data have been provided by the French meteorological office, Météo France. For the year 2003, for instance, the mean swell observed around Tahiti (at four points at 17°S and 18°S latitude and 149°W and 150°W longitude) is 2.2 m high and the mean period is 10.6 s. However, much stronger swell episodes occur several times in the year and may lead to waves up to 4 m high in the Society archipelago and up to 6 m high in the Austral, the southernmost archipelago, during the austral winters. Such strong *Hs* events can be disastrous for infrastructure and can seriously disturb the local marine transport. Moreover, swell events are of particular importance on atolls whose elevation of generally only a few metres is often lower than the wave height. The quantification and the forecasting of these swell episodes are, therefore, vital for French Polynesia.

Background seismic noise occurs over the whole seismic spectrum, that is, comprising frequencies of several tens of hertz to a few mHz. Swell makes a contribution to the seismic signal in two distinct period ranges, corresponding to different origins. A major peak in the seismic noise related to swell is present worldwide between periods of 1 and 10 s, centred near 5 s. This peak is called the "double frequency peak' (hereafter called the DF peak) since it is generally centred on twice the swell frequency. It is classically interpreted as having been generated by standing waves resulting from the interaction of swells with similar periods but travelling in opposite directions (e.g. Longuet-Higgins 1950; Hasselmann 1963; Cessaro 1994). The DF peak has been used to deduce swell characteristics, in particular from inland seismic stations along the Atlantic and Pacific coasts of the United States (e.g. Bromirski *et al.* 1999; Bromirski 2001). The second, less energetic peak related to swell activity is called the 'single frequency peak' (hereafter called the SF peak) and is in the same frequency band as swell (periods between 10 and 20 s). This SF signal, which is the subject of this paper, is widely accepted to be generated by the swell-induced pressure variations on the shallow seafloor in coastal areas (e.g. Hasselmann 1963). Due to its smaller amplitude, especially at inland continental stations, the SF peak has been historically less well studied than the DF peak. From data recorded at stations installed on small islands such as in French Polynesia, we show, however, that the SF peak is well developed and that, in such an environment, more information can be extracted from the SF than the DF peak. Indeed, the ground motion induced by the swell in the period range 13–20 s has been shown to produce a coherent signal (e.g. Talandier & Hyvernaud 1991), which is strongly correlated between islands and correlated with the swell amplitude itself. Moreover, the SF peak is linearly polarized, enabling one to estimate the swell direction from its polarization properties. Conversely, the DF peak for French Polynesian islands never shows any state of polarization. In the remainder of the paper, we use the term swell-related seismic noise (SRSN) to refer to the island vibrations excited by the oceanic swell in the SF band.

In the second section of this paper, we describe the seismic network from which the seismic data are taken. In the third, we discuss the seismic spectra and describe the SF peak, we outline the method used to determine the polarization and we discuss the nature of the SF signal. We then, in the fourth and fifth sections, develop a method of analysis of the SF signal to obtain quantitative values of the swell amplitude and azimuth. This enables us to test the relative ability of the seismic stations running in French Polynesia to provide direct and reliable parameters to quantify the swell amplitude and azimuth. To achieve this, we analyse data recorded during two periods of typical southerly (2002 August and September) and northerly swells (2003 January) at a number of temporary and permanent stations. We also analyse the data recorded over the whole year 2003 at the permanent long period seismic station PPTL installed in Tahiti, and we show that data from this seismic observatory can potentially be used to monitor long-term (decadal) wave activity and its variation with climate changes (e.g. Grevemeyer *et al.* 2000). In the sixth and final section we investigate whether infrasonic data from a mini-array in Tahiti can be used to give a further independent estimate of the swell amplitude.

2 SEISMIC STATIONS IN FRENCH POLYNESIA—DATA ACQUISITION

The PLUME network consists of 10 seismic stations that were running in French Polynesia between 2001 November and 2005 August to record the local and remote seismicity (Barruol *et al.* 2002). The primary aim of PLUME is to determine the upper mantle structure and dynamics beneath this area (e.g. Fontaine *et al.* 2002; Maggi *et al.* 2003; Barruol *et al.* 2004), and particularly their relation to hotspot activity. This network has enabled us to investigate hydroacoustic *T* waves (e.g. Talandier *et al.* 2002) as well as to detect and localize the local and regional seismicity (Reymond *et al.* 1991; Hyvernaud *et al.* 1993). The geographical distribution of PLUME stations (Fig. 1 and Table 1) was designed to complement the distribution of the existing permanent seismic network, composed of three long-period seismic stations managed by the *Laboratoire de Géophysique* of the *Commissariat à l'Energie Atomique* (hereafter called LDG/CEA), and by the Incorporated Research Institution for Seismology (IRIS) broad-band stations PTCN on Pitcairn island and RAR in Rarotonga (Cook islands). The PLUME network covers an area of more than 2 000 000 km^2.

The seismic stations installed for the PLUME experiment consist of broad-band Streckeisen STS-2 sensors, which have a flat response between 0.01 and 5 Hz. They record continuously, on two independent channels, at rates of 40 and 1.25 samples per second. The

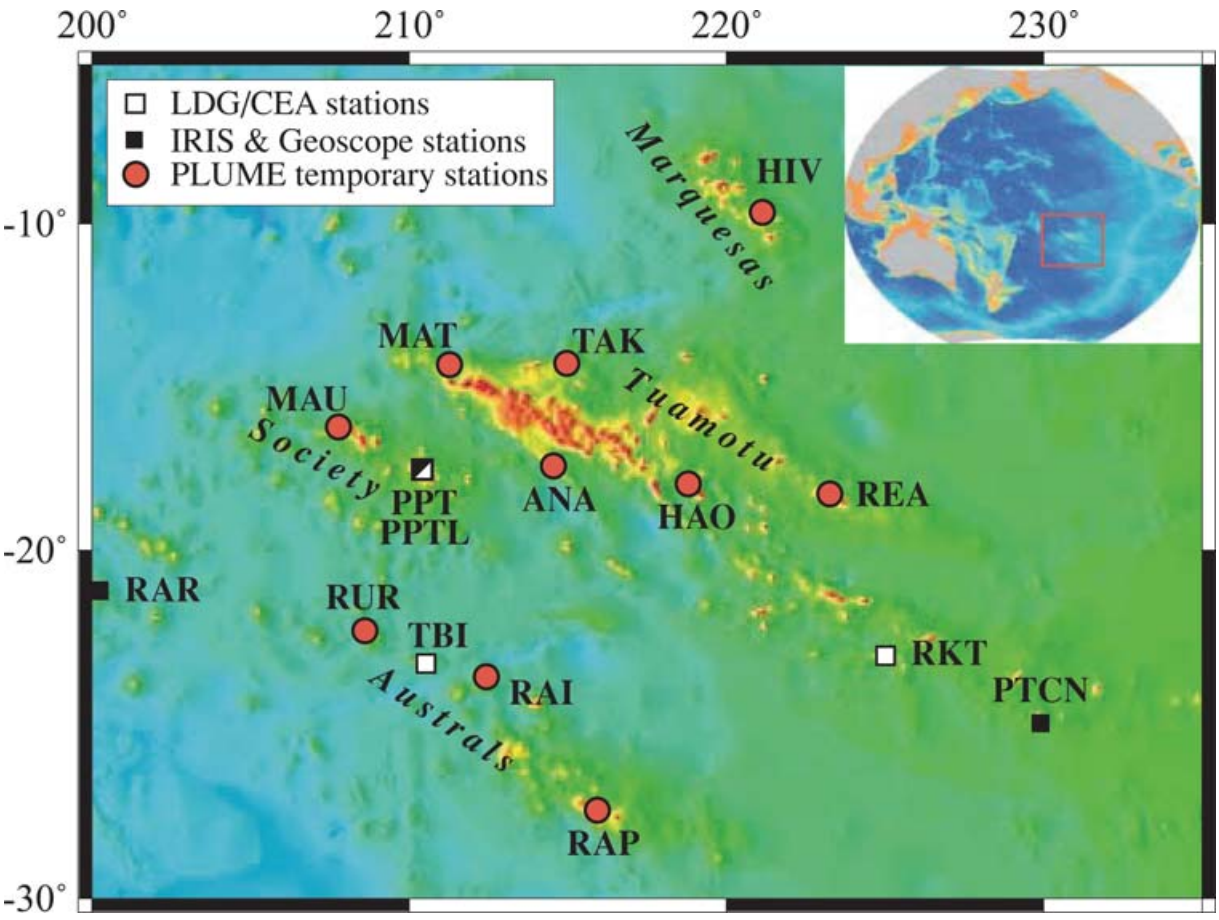

Figure 1. Bathymetric map of French Polynesia with the location of the PLUME (circles), LDG/CEA (white squares), IRIS and Geoscope (black squares) seismic stations.

Table 1. Stations location, network, island and archipelago.

Station	Network	Lat (°)	Long (°)	Island &Archipelago
ANA	PLUME	−17.354	−145.505	Anaa, Tuamotu
HAO	”	−18.058	−140.957	Hao, Tuamotu
MAT	”	−14.869	−148.707	Mataiva, Tuamotu
REA	”	−18.458	−136.440	Reao, Tuamotu
TAK	”	−14.471	−145.036	Takaroa, Tuamotu
MA2	”	−16.443	−152.274	Maupiti, Society
MAU	”	−16.423	−152.238	Maupiti, Society
HIV	”	−9.7590	−139.004	Hiva Oa, Marquesas
RAP	”	−27.618	−144.334	Rapa, Austral
RAI	”	−23.873	−147.685	Raivavae, Austral
RUR	”	−22.426	−151.368	Rurutu, Austral
TBI	LDG/CEA	−23.350	−149.460	Tubuai, Austral
RKT	”	−23.118	−134.972	Rikitea, Gambier
PPTL	”	−17.569	−149.576	Pamatai, Tahiti
PPT	Geoscope	−17.569	−149.576	Pamatai, Tahiti
RAR	IRIS	−21.210	−159.770	Rarotonga, Cook
PTCN	”	−25.073	−130.095	Pitcairn, Gambier

first channel is primarily dedicated to body wave analysis while the second one is dedicated to surface wave analysis. For the present SRSN analysis, we undersampled the 40 Hz channel at 10 Hz.

The long period LDG/CEA permanent stations (Fig. 1) are installed in Tahiti, Tubuai (Austral islands) and Rikitea (Gambier islands). They are equipped with 60 s long-period velocity sensors designed by LDG/CEA, which sample the data at 4 Hz. The Tahiti station PPTL is part of the CTBT (Comprehensive Nuclear Test Ban Treaty) organization network. This station was certified several years ago on criteria including noise level, seismic vault construction, energy, 24-bit digitizer, and good horizontal seismometer orientation. This station is, therefore, of high quality and has been running for more than 30 yr.

Instead of analysing the whole PLUME data set in order to determine how accurately one can determine swell heights and azimuths from the seismic data, we focus mainly on certain periods, those characterized by strong swell, or a succession of quiet and strong swell episodes. The first period is 2002 August to September (austral winter), when swell generated in the southern Pacific crossed French Polynesia. A particularly strong swell affected French Polynesia on 2002 August 4, estimated at 3.4 m around Tahiti by satellite altimetry. The second period is 2003 January (boreal winter), during which several swell episodes were generated by severe storms in the northern Pacific. Strong swell events (3–4 m high) arrived in French Polynesia from the NW on 2003 January 14 and 24. By analysing data from these two periods, we aim to characterize North and South swells. For the third period selected, 2003 April–May, which encompasses a swell event of reported height 3.7 m, we make a combined analysis of seismic and infrasonic data recorded on Tahiti island. This analysis provides information about the origin of the swell-related acoustic noise and the ability of microbaroms to monitor independently the ocean activity.

3 MICROSEISMIC NOISE IN FRENCH POLYNESIA

3.1 Seismic noise spectral analysis: mean levels

In order to quantify the noise amplitude in the various frequency bands and to investigate its origin, it is necessary first to analyse the spectrum of ground motion at each seismic station. We consider periods ranging between 0.1 s and several hundreds of seconds in the case of the broad-band sensors available in French Polynesia. In order to obtain statistically significant values of the mean noise level at the different seismic stations, we compute the spectra at each station by selecting 30 min of data each day with a sampling rate of 10 Hz for the PLUME stations and 4 Hz for the LDG/CEA stations, and then average the spectra for the selected periods (2002 August–September and 2003 January). Since our aim is to characterize the seismological noise (i.e. all the non-earthquake ground vibration) over the whole spectrum, seismic events of magnitude larger than 5.5, as determined by the National Earthquake Information Center (NEIC), are rejected.

The power spectral density functions (PSD) are calculated for each 30 min series. We use a Hanning taper to minimize the border effects and perform a deconvolution to remove the instrument response. Also, the signals are pre-whitened. The fast Fourier transform of each time series is then computed. The PSDs are obtained by computing the square of the spectral amplitude divided by the time series length (e.g. Aki & Richards 1980) and are converted to decibels (dB) with respect to acceleration. An arithmetic smoothing of the spectra is used to achieve statistical consistency (Chave *et al.* 1987) with a moving, three-point smoothing window centred on the current index. PSDs of the 30 min series are finally averaged, component by component, for each of the selected periods. These averaged PSDs are plotted together with the 'high noise' and 'low noise' models determined by Peterson (1993) in his systematic analysis of noise at the IRIS permanent seismic stations.

To illustrate the noise amplitude observed at the temporary and permanent stations, we present in Fig. 2 a selection of PSDs obtained at temporary and permanent stations for the period 2002 August–September (a) and 2003 January (b). The whole set of spectra may be found on the PLUME web site (http://www.dstu.univ-montp2.fr/TECTONOPHY/polynesia).

The PSDs have several general features, which are independent of the station and the time of year. On the high frequency side of the spectra, the noise gradually increases from 1 to 10 Hz. This is generally accepted to be caused by local winds, trees and human activities. Below 1 Hz, the noise smoothly increases as the DF peak, typically about 0.2 Hz, is approached. As mentioned above, this peak (white arrow in Fig. 2), close to double the ocean wave frequency, is classically interpreted in terms of non-linear interactions between waves travelling in opposite directions (Longuet-Higgins 1950) whereby elastic waves which propagate as fundamental Rayleigh waves in the ocean seafloor are generated. Such standing waves may develop within or near oceanic storms or may result from coastal wave reflection. The steep decline of the PSD on the lower frequency side of the DF peak is due to the rarity of waves with periods longer than 20 s (Webb 1998). At longer periods, a smaller peak centred between 0.05 and 0.07 Hz is visible at most stations. This peak (grey arrow in Fig. 2) is the SF peak mentioned above, associated by Hasselmann (1963) with the conversion of swell energy into elastic waves via the continuous regime of pressure variations on the external slopes of the island (e.g. Hasselmann 1963; Kibblewhite & Ewans 1985; Hedlin & Orcutt 1989). The SF peak is best visible at insular or

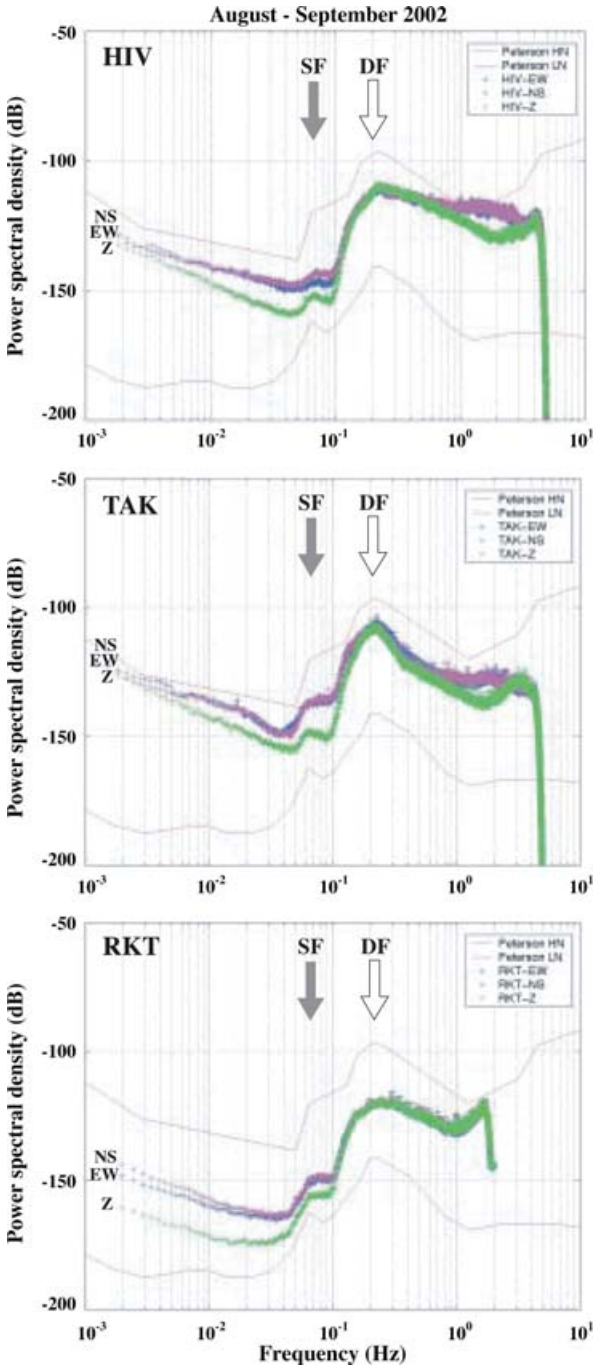

Figure 2. Power spectral density (PSD) of few selected PLUME and LDG stations during (a) the austral winter (2002 August–September) and (b) the austral summer (2003 January). For each period are shown two PLUME noise spectra and one LDG/CEA spectrum (RKT and PPTL). The three components (NS, EW, Z) are plotted separately. Note the presence of the 'single frequency peak' close to 0.06–0.07 Hz, identified by the grey arrow and 'SF' and corresponding to the SRSN (swell-related seismic noise). The 'double frequency peak' around 0.2 Hz is marked by a white arrow and 'DF'. The two continuous lines correspond to Peterson's (1993) high and low noise model (HNM and LNM). Note also that at the 'SF' peak, the noise level of the vertical component is about 5 times smaller than that of the horizontal ones; this suggests a quasi-horizontal ground motion in this frequency range. The PSD highest frequency is limited by the signal sampling frequency: we used 40 samples per second for MAT, 10 samples per second for HIV, TAK and REA and 4 samples per second at the LDG/CEA stations RKT and PPTL.

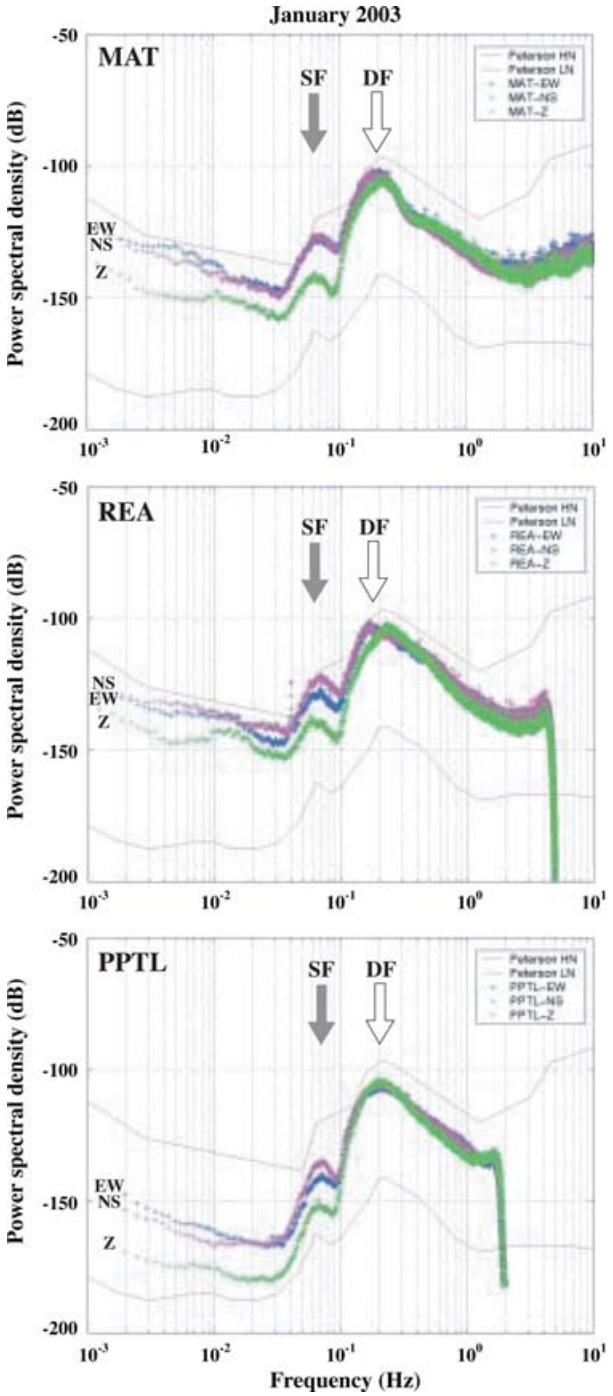

Figure 2. (*Continued.*)

coastal stations but has also been observed at continental stations (Peterson 1993; Stutzmann *et al.* 2000) and on the ocean bottom (e.g. Beauduin & Montagner 1996). As the period increases, after a noise minimum in the range 20–30 s, called the 'noise notch' by Webb (1998) and reported to be a world-wide feature, the noise level increases gradually toward the long period signals. At periods longer than 30 s, the noise is likely to be dominated by infragravity waves (e.g. Webb 1998) and atmospheric pressure variations (Sorrels 1971; Sorrels *et al.* 1971; Müller & Zürn 1983; Zürn & Widmer 1995).

Fig. 2 shows that the three components of the PSD behave differently depending on the frequency: at frequencies above 0.1 Hz, the three components have similar amplitude of seismic noise. At the DF peak, the similar amplitude of the three components suggests that the signal is not polarized. At frequencies below 0.1 Hz, the amplitude of the vertical component is systematically less (by a factor of approximately 5) than the amplitude of the two horizontal components. Thus in the SF band, that is, between 10 and 20 s, the PSD analysis shows that the swell interacting with the shore induces vibrations primarily contained within the horizontal plane.

Comparing the PSDs obtained at the LDG permanent stations (PPTL, RKT) and at the PLUME temporary sites confirms that the LDG permanent installations give better quality data in general over the whole seismic spectrum. The island stations' noise spectra at high frequencies (above 0.1 Hz) resemble each other, as do the temporary PLUME stations' (Fig. 2) and all are rarely above the high noise level of Peterson (1993). The comparison of the PLUME station noise levels with the noise level of permanent insular Geoscope stations (Stutzmann *et al.* 2000) suggests that some of the PLUME temporary installations give horizontal data with similar noise levels to those of permanent installations in oceanic or coastal environments.

3.2 Swell front detection from time–frequency analyses

If averaging spectra over time provides information on the mean noise characteristics and thus mean swell height during a given period, then following the spectral variations with time may allow the detection and tracking of swell arrivals. As an example, we analyse data from PPTL station for the period 2004 January 13 to 18. During this period, French Polynesia experienced an exceptional succession of several NNW incoming swells, each about 3 m high, as deduced from NOAA 'WaveWatchIII' wind-derived models. The temporal spectral variation of the PPTL North component is presented Fig. 3.

Three successive dispersed swell arrivals are visible in the spectrogram in Fig. 3, indicated by the dashed lines (a, b and c) and characterized by linear, oblique packets of long period energy. For each swell event, one observes the very low frequency waves (21–22 s period) arriving first, and then a progressive shift of the energy towards higher frequencies, due to the fact that gravity waves are dispersive, that is, long period waves travel faster than short period waves. Time–frequency analysis provides one way to identify several simultaneous swell arrivals: this can be seen for instance in Fig. 3 on 2004 January 18, when two swells (b and c) are clearly distinguished by their spectral content. However, this method, which utilizes the data from only one station, cannot provide any information about the swell azimuth. In order to investigate the swell azimuth, complementary analysis of the particle motion is developed in the next section.

3.3 Seismic data processing: method of polarization analysis

All the PSDs calculated at the French Polynesian island seismic stations are characterized by a clear SF peak in the range 0.05–0.09 Hz (i.e. periods between 11 and 20 s). As this band corresponds to typical swell frequencies, we focus on this part of the spectrum in order to be able to quantify, in subsequent sections, how this swell-related microseismic noise can provide useful information on the wave height and swell direction. In the subsequent discussion in this section, and in order to restrict our investigation to periods in the range 13–20 s to avoid any contamination of the SF band with the DF band, we apply a sixth order Butterworth bandpass filter to the data with corner frequencies of 0.05 and 0.077 Hz.

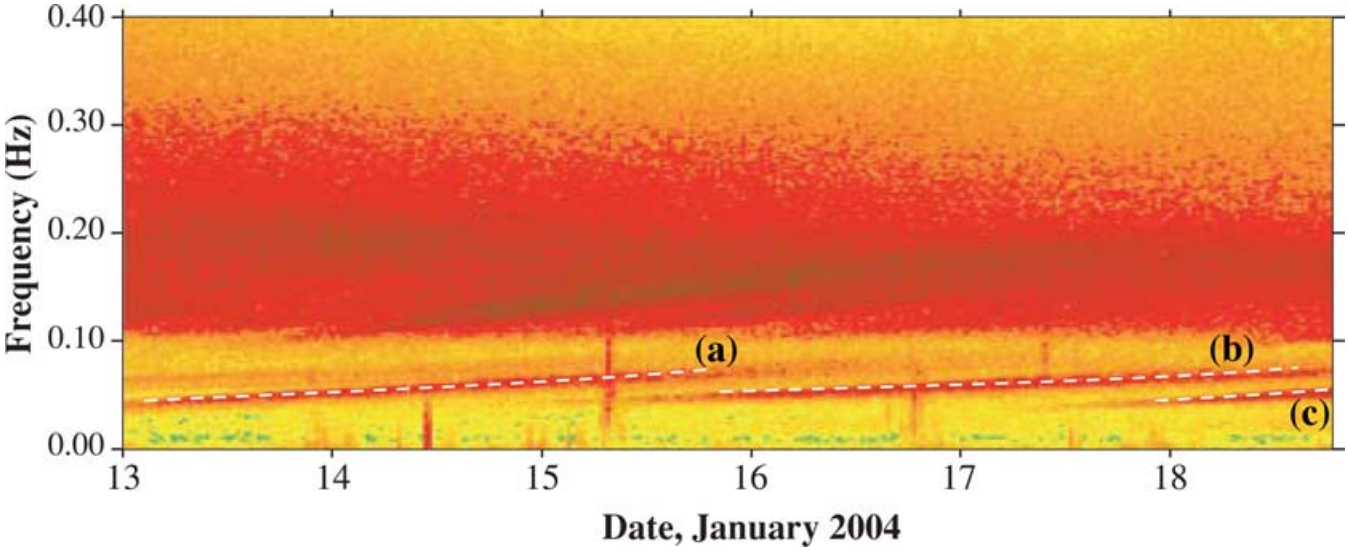

Figure 3. Temporal spectral variation of the seismic data recorded at station PPTL on Tahiti island between 2004 January 13 and 18. Three successive swells crossed French Polynesia during this period (white dashed lines a, b and c). They are characterized by long period waves (around 20 s). The oblique trend of each long period signal clearly shows the dispersion, with long period waves travelling faster than short period waves.

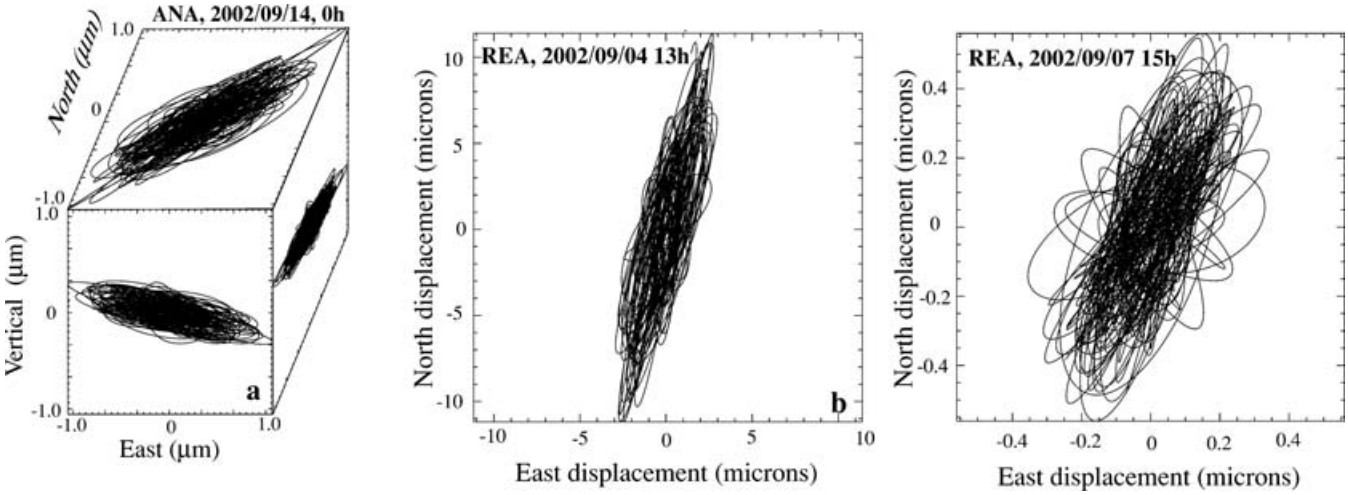

Figure 4. Examples of ground particle motion of 30 min of signal that allow to determine the noise amplitude (length of the ellipse) and azimuth (azimuth of the ellipse major axis). (a) 3-D representation of the microseismic noise at ANA on 2002 September 14, showing a clear horizontal polarization (total amplitude around 2 μm) and little vertical displacement. The swell-related seismic noise (periods in the range 13–20 s) is essentially in the horizontal plane. (b) Example of 30 min of the horizontal ground motion recorded at station REA in the eastern Tuamotu during a swell episode on 2002 September 4, showing a strong polarization (total amplitude 20 microns). (c) Horizontal ground motion at REA, during a quiet swell episode on 2002 September 7, (note that the total amplitude has decreased to less than 1 micron).

As noted above, the amplitudes of the horizontal components of the PSDs in the SF band are generally larger than the vertical component by roughly a factor of 5. The SRSN appears, therefore, to be contained mainly within the horizontal plane. This can be seen in the 30 min seismic record filtered between 0.05 and 0.077 Hz in Fig. 4(a). In this figure, the 3-D swell-induced ground particle motion is small along the vertical direction and is primarily contained within the horizontal plane. It is also elliptical in shape. The major axes have strong preferred directions and the ellipses are more elongated during swell episodes (Fig. 4b, amplitude of approximately 20 microns on 2002 September 4) and are more randomly oriented and/or have a small elongation ratio during quiet swell episodes (Fig. 4c, right, amplitude of 1.0 micron on 2002 September 7). This visual analysis of the ground particle motion at the SF peak illustrates that the swell induces an approximately linear and horizontal particle motion. A more detailed geometrical analysis of the waves and their attenuation is presented in the following sections of the paper and argue that the studied waves have not the characteristics of Rayleigh waves, as commonly described at continental (e.g. Haubrich & McCamy 1969; Cessaro 1994; Schulte-Pelkum *et al.* 2004) and on ocean bottom stations (e.g. Barstow *et al.* 1989; Webb 1998).

In order to extract from these elliptical ground particle motions the amplitudes and the directions of the swell-related microseismic noise, we developed two methods to determine the length and the azimuth of the major axis of the ellipse. The first method is geometric: by successive rotation of the two horizontal components, we perform a grid search of the direction for which the amplitude

of one component is maximum while being minimum for the other component. This allows determination of the azimuth and the maximum amplitude of the noise in the selected time window. The second method is based on principal component analysis (PCA) (Pearson 1901; Hoteling 1933). It characterizes the 3-D elliptical ground motion by resolving the data into three components as East, North and Vertical. PCA is performed on the covariance matrix:

$$Cjk = \frac{1}{Np} Y^T Y,$$

where Np is the number of points in the time window and Y is a $[Np \times 3]$ centred matrix with the components (East, North, Vertical up) as its columns, and Y^T is the transpose of Y. Y is mean centred by column:

$$Yij = (Yrawij - \overline{Yrawj}).$$

Yraw is a matrix of the original data with the three components (East, North, Vertical up) as its columns; i denotes rows, j denotes columns, and $\overline{Yrawj}$ is the mean of each column.

C is symmetrical so that we can always determine its eigenvalues λ^j and eigenvectors $\mathbf{a}^j$. The azimuth, θ is given by the direction of eigenvector a^1, corresponding to the maximum eigenvalue, λ^1:

$$\theta = \arctan \frac{a_2^1}{a_1^1} \qquad \text{for} \quad \lambda^1 > \lambda^2 > \lambda^3 ,$$

where a_2^1 and a_1^1 are the cartesian coordinates of a^1 in the horizontal plane. The incident angle, *Incid*, is obtained in the same way:

$$Incid = A \cos\, a_3^1.$$

Since the incident angle varies in the range [0°–180°], its slope is signed in order to remove the 180° ambiguity on the swell azimuth: if the incident angle has no meaning for Rayleigh waves (elliptical particle motion in the vertical plane), and if it always takes the value 0 or 180° for Love waves (pure linear horizontal motion perpendicular to the direction of propagation), it is valuable information for P waves (pure linear polarization, with the constraint of a radial vector always pointing toward the surface). Curiously, a fact that is not yet explained, the linear SRSN motion is not exactly horizontal but systematically dips slightly toward the direction of propagation, that is, the sign of the incident angle is opposite to that of P waves. We have used this property to remove the 180° ambiguity in the swell azimuth.

Once we have the principal directions, we are able to obtain the major axis, L, by the following projection: $L = \cos(\theta)\, N + \sin(\theta)\, E$, where N and E are the north and the east components, respectively.

The eigenvalues are used to compute the coefficients of polarization: these coefficients range from 0 to 1 and characterize the degree of planarity and linearity of a plane wave, a value of 1 corresponding to a purely planar or linear motion. The coefficients of polarization are defined as follows:

$$CpH_{(N,E)} = \sqrt{1 - \frac{\lambda_{\min}^{NE}}{\lambda_{\max}^{NE}}},$$

is the coefficient of polarization in the horizontal plane. A value of 0 indicates no preferred direction of motion in the horizontal plane and a value of 1 indicates pure linear particle motion in the horizontal plane.

A projection of the $\{N, Z, E\}$ components onto the incident plane, that is, the vertical plane containing the L and Z components, enables us to compute a vertical polarization coefficient, *CpZ*, in the same way as for *CpH*, except that the components $\{L, Z\}$ are used instead of {N, E}:

$$CpZ_{(L,Z)} = \sqrt{1 - \frac{\lambda_{\min}^{LZ}}{\lambda_{\max}^{LZ}}}.$$

A *CpZ* value of 1 indicates linear particle motion in the vertical plane (as for P or Love waves, for instance) whereas a value close to 0 indicates an almost circular particle motion (i.e. Rayleigh wave).

$CpLin_{(N,Z,E)} = \sqrt{1 - \dfrac{(\lambda^2 + \lambda^3)}{2\lambda^1}}$ is the coefficient of linearity.

These parameters enable us to quantify the polarization of the SRSN. We are also able to discriminate between pure polarized noise and true earthquake signals by considering the incident angle. Our measurements show that the swell-related signal is indeed primarily contained within the horizontal plane, having polarization coefficients *CpZ* in the range 0.8–1.0 (and even between 0.95 and 1.00 at the high quality PPTL permanent station) and *CpH* in the range 0.6–1.0.

The amplitudes and the azimuths determined by both methods (geometric and PCA) give very similar results. However, PCA is much faster in calculations and gives more information about polarization than the geometric method. Consequently, we use PCA in the subsequent analysis.

In summary, the swell-related noise measurements are performed on data filtered between 0.05 and 0.077 Hz (i.e. periods 13–20 s). We use 30 min of data each hour, leading to one value of the two parameters (amplitude and azimuth) per hour. This allows us to statistically remove bad events resulting from noise other than that originating from swell (e.g. small seismic events, glitches or artefacts in the data). The hourly sampling allows us to date swell arrivals at a given station with good precision and potentially to track swell propagation between several stations.

3.4 Nature of the SF signal

To illustrate the technique described in the previous section, to discuss the signal characteristics, and to justify our choice of using the SF instead of the DF peak, we present in Fig. 5 the particle motion analysis obtained at the temporary stations MAT and TAK and the permanent station PPTL during the month of 2003 January, when several swell fronts crossed French Polynesia. The data set, composed of a 30 min record each hour, is analysed around the SF peak (filtering the data to pass 0.045–0.075 Hz) and also around the DF peak (filtering to pass 0.1–0.4 Hz). The results obtained in this manner are compared with swell observations provided by Météo France. From synoptic maps incorporating visual observations together with satellite altimetry, Météo France provides a daily value of the swell height and period around Tahiti. Two long period swells (>13 s) occurred on January 14 and 24, of height 2.5 and 3.0 m, respectively. Our results (Fig. 5) show several important features:

(i) In the SF band, the microseismic noise has two prominent peaks, on January 14 and 24, which is evidence for the good correlation between the long-period swell events deduced by satellite altimetry and the microseismic noise in this frequency band.

(ii) The noise amplitude is systematically lower for the SF (lower curve) than for the DF peak (upper curve), in agreement with the PSD analysis.

(iii) There is no correlation between the SF and DF curves, suggesting independent origins. For instance, the swell occurring on January 14 generates a strong peak in the microseismic noise at the

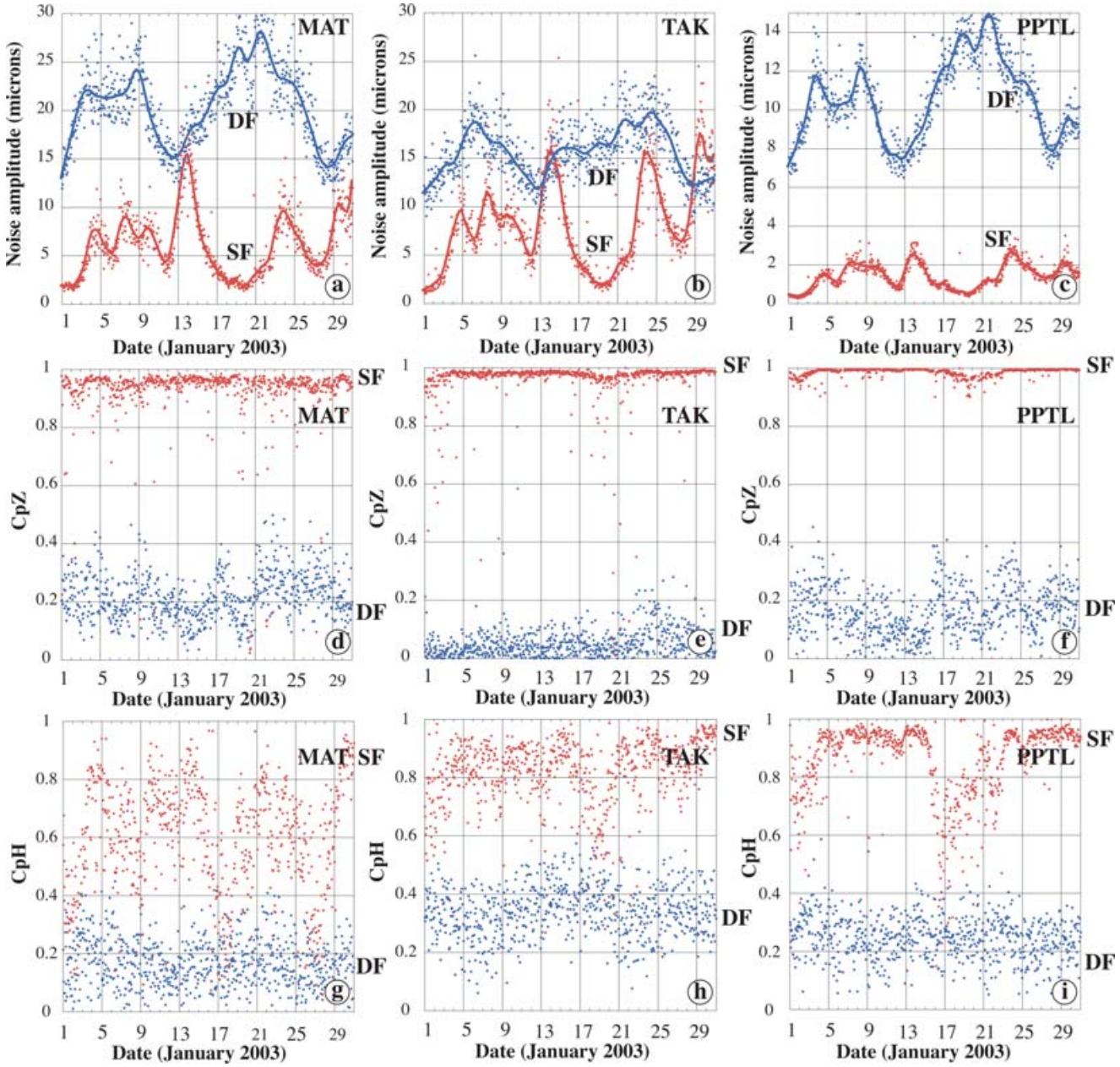

Figure 5. Microseismic noise amplitude variations (in microns), for the period range 2.5–20 s, measured at MAT (a), TAK (b) and PPTL (c) in 2003 January. On each diagram, we separate the measurements made in the SF band (0.045–0.075 Hz, red points) and in the DF band (0.1–0.4 Hz, blue points). From (d) to (i), are presented the geometrical analysis of the ground motion related to the SF and to the DF band at the three stations. (d), (e) and (f): temporal variation of *CpZ* (coefficient of polarization in the vertical plane). A value close to 1, as observed for the SF peak, means the ground motion is almost linear in the vertical plane whereas a value close to 0 indicates a more circular displacement. (g), (h) and (i): temporal variation of *CpH* (coefficient of polarization in the horizontal plane). Here also, a value close to 1 indicates a linear motion in the horizontal plane and a value close to 0, as for the DF signal, indicates a circular motion. See text for comments and interpretation.

three stations in the SF band but is associated with low noise levels in the DF band. Conversely, the quiet swell episode occurring between January 17 and 21 corresponds to a high DF noise period at MAT and PPTL.

(iv) The microseismic noise amplitude in the SF band appears to decrease with the distance from the shore: MAT and TAK which are both installed on atolls, close to the reef (100 to 300 m distant) have similar SF noise amplitudes (15 microns for the January 14 event) whereas PPTL (installed at several km from the reef) has a similar qualitative SF series but the amplitude is much lower (around 3 microns for the January 14 event). Such signal attenuation may explain why we do not observe a clear SF noise amplitude at the PLUME stations HIV and RAP both of which are located several km from the coast on the islands of Hiva Oa and Rapa, respectively. The absence of coral reef around these islands and the indented coastal geometry are also factors that might affect the signal structure.

(v) The particle motion analysis demonstrates that the ground motion in the SF peak is linearly polarized: in the 0.045–0.075 Hz band, the *CpZ* values (Figs 5d–f) are very close to 1 and the *CpH* values (Figs 5g–i) are generally larger than 0.6 (at MAT), and even

0.8 (at TAK and PPTL), indicating a linear and horizontal ground motion. On the other hand, the ground motion in the DF band (0.1–0.4 Hz) is not polarized: both *CpZ* (Figs 5d–f) and *CpH* are lower than 0.4, suggesting a random ground motion in this frequency band. These examples demonstrate that no preferred direction of motion can be extracted from a particle motion analysis in the DF band while the ground motion associated with the SF peak is linearly polarized in the horizontal plane and, therefore, carries some directional information.

Our measurements show that the SF signal is characterized by a quasi horizontal and linear particle motion. The well-defined linear polarization in the incident plane ($CpZ > 0.9$) and in the horizontal plane ($CpH > 0.6$ or 0.8) is not compatible with Rayleigh waves for which the particle motion is retrograde elliptical in the vertical plane. The linear polarization and the quasi-horizontal particle motion observed on the SF signal could be compatible with Love waves, but the direction of propagation is perpendicular to the Love wave polarization direction. The SF signal does not, therefore, have the geometrical characteristics of surface waves. From its linear polarization properties, and since we never observe SRSN with SH properties excluding their possible shear wave nature, the SRSN could correspond to sub horizontal *P* waves, with the restriction that the sign of the slope of the incident angle is always the opposite to that observed for *P* waves. The linear polarization direction is indeed not exactly horizontal but is slightly inclined toward the propagation direction.

As mentioned above, the SRSN appears to be quickly attenuated as the distance from the reef increases. In order to quantify the influence of the distance from the 'active' reef to the seismic station on the SF microseismic noise amplitude, we use data from two one-component LDG/CEA seismic stations running on the same atoll to test the effects of southerly and northerly swell on the SF peak amplitudes. Stations VAH and PMOR (Fig. 6a) are installed at about 30 km from each other, on, respectively, the southern and northwestern rim of the Rangiroa atoll (northern Tuamotu), one of the largest atolls in the world (more than 60 km long). The comparison of the respective PSDs for a given swell arriving from the south (on 2003 April 30, Fig. 6b) clearly shows that the southern station VAH (a few hundreds of metres from the 'active' barrier) has a SF peak of about one order of magnitude higher than the northern station PMOR, which is farther from the 'active' reef. On the other hand, we observe the opposite behaviour for a northerly swell event (on 2004 January 14, Fig. 6c): the northern station PMOR has a clear SF peak which is an order of magnitude stronger than that observed at the southern station VAH. The above observations, deduced from two stations installed on the same island, demonstrate that the SF signal is strongly attenuated over short distances. Such attenuation could explain the difference in noise amplitude between ANA and REA (Fig. 7) but may also explain the much lower SF amplitude observed at PPTL (a few km from the shore) compared to MAT or TAK, installed at a few hundreds of metres from the reef (Fig. 5). These observations provide a supplementary argument against the Rayleigh or Love nature of the waves analysed in this SF band. Surface waves are not expected to be so greatly attenuated over such short distances.

In summary, the SF noise analysed in this study has strong similarities with horizontally–propagating *P* waves. Our findings appear to be related to the oceanic environment combined with the small sizes of the islands and perhaps to the steep bathymetry. They cannot be extrapolated to continental environments where a number of previous microseismic noise analyses have demonstrated that the waves in the SF band propagate primarily as Rayleigh waves (e.g. Haubrich & McCamy 1969; Cessaro 1994; Shapiro *et al.* 2005).

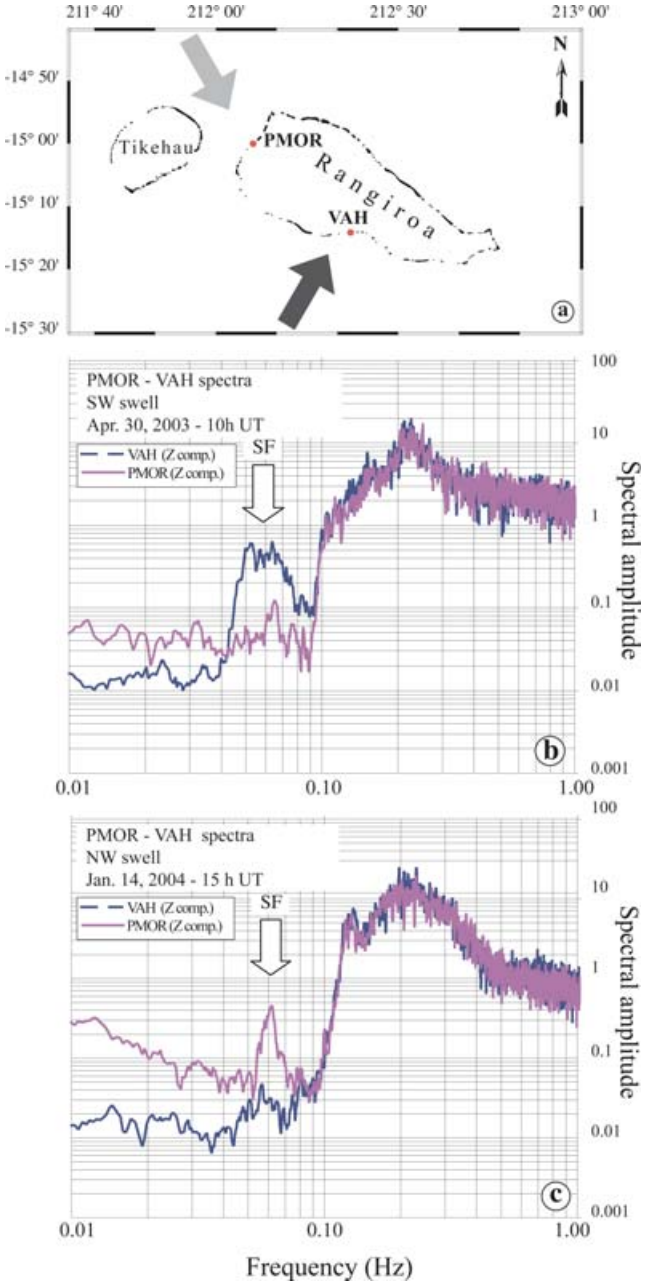

Figure 6. Noise spectral amplitudes observed at two stations operating on the same island ((a) station location on Rangiroa atoll, Tuamotu) for southerly (b) and northerly (c) swells. For these two swell events (occurring respectively on 2003 April 30 and 2004 January 14), the peak in the SF frequency is much more developed at the station close to the 'active' reef, suggesting that the SRSN is rapidly attenuated across the atoll.

4 QUANTIFICATION OF SWELL AMPLITUDE FROM MICROSEISMIC NOISE

In this section, we demonstrate in a few steps that the microseismic noise in the SF band recorded at the various seismic stations is directly induced by swells. First, by a simple calculation, we show

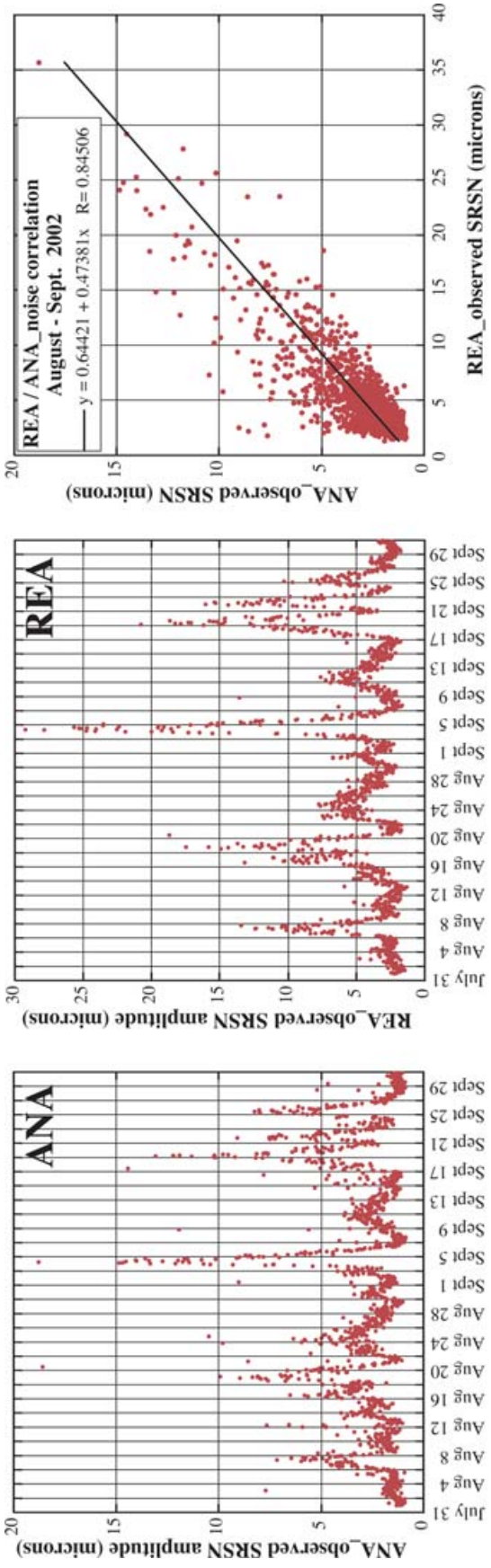

Figure 7. Microseismic noise amplitude variations (in microns), for the period range 13–20 s, measured at ANA and REA in 2002 August–September. The similarity of the plots (except some differences in amplitude) for stations separated by several hundreds of kilometres suggests that the distance to the source (i.e. the origin of the swell event) is much greater than the distance between the stations. The noise correlation between the different stations is shown on the right and the linear regression fit has a high correlation coefficient ($R = 0.84$). The absence of an obvious time lag between the microseismic noise peaks recorded at the two stations can be explained by the fact that swell fronts arriving from the SW during the austral winter reach ANA and REA roughly simultaneously.

that the actual SRSN amplitude can be explained by the estimation of the pressure variation along the external slope of the shore. Secondly, we show that SRSN measured at seismic stations separated by several hundreds of kilometres has very similar variations in time. In the following two subsections we present the wave predictions provided by the NOAA (National Ocean and Atmospheric Administration) ocean 'WaveWatch' model and we compare the predicted swell height with the SRSN observations. We show that the observed SRSN is strongly correlated with the wave heights predicted by the 'WaveWatch' model. We then focus on the permanent station PPTL in Tahiti and analyse the data for the whole year 2003 in order to define the transfer functions that relate the measured seismic noise to the swell height. We finally show that the Tuamotu is a barrier to swell and might be the source of discrepancies between observed and predicted swell heights.

4.1 Theoretical and observed seismic noise amplitude

Before discussing in greater details the swell–SRSN relationships, it is important to discuss where and how the SF noise originates and whether the amplitude of the ground vibration is of the same order as that which can be theoretically expected.

As mentioned above, the primary microseismic noise (the SF peak) is generally accepted to be generated by the pressure variation applied to the ocean bottom by the swell vertical fluctuations. This noise amplitude depends on the swell wavelength λ and on its amplitude (Hasselmann 1963). It is also commonly accepted that the travelling wave interacts with the seafloor when the water depth h is less than about half of the swell wavelength (e.g. Darbyshire & Okeke 1969). This wavelength can be approximated to $\lambda = gT^2/2\pi$, T being the swell period and g the gravitational acceleration. Swells of period between 13 and 20 s will, therefore, have wavelength ranging between 260 and 624 m. Although the parse coverage in multibeam-derived bathymetry around the Polynesian islands (Jordahl *et al.* 2004), the punctual depth sounding and the multibeam-derived bathymetry around the Society islands show that the external slope of the barrier reef is steeply inclined toward the deep ocean, of the order of 45° (e.g. Rancher & Rougerie 1995; Bonneville & Sichoix 1998; Clouard & Bonneville 2004). This implies that the SRSN is generated at less than 150 to 300 m from the emerged reef for swell periods of, respectively, 13 and 20 s. Such small distances suggest that the SF signal observed on atolls may be generated very close to the seismic station itself, less than 1 km for the atoll sites. This observation is apparently in contradiction with previous explanations favouring the presence of large areas of shallow water around the island for the excitation of microseisms in the SF peak (e.g. Hasselmann 1963; Hedlin & Orcutt 1989). However, as explained below, the distance of the seismic station from the noise source area is also an important factor which may control the SF noise amplitude.

We now attempt to quantify the magnitude of the theoretical ground motion associated with a given swell height for typical period ranges, assuming that the swell-induced noise is created by the swell-induced pressure oscillation on the ocean bottom in the vicinity of the shore. Our approach is to determine first the pressure fluctuation induced by the swell on the ocean bottom and then to deduce the ground displacement related to this pressure variation.

The pressure fluctuation at the ocean bottom is linked to the surface fluctuation by:

$$P(h) = \frac{P_0}{\cosh(kh)}, \tag{1}$$

where P_0 is the pressure at the surface, k the swell wave number ($k = 2\pi/\lambda$) and h the water depth (e.g. Bromirski & Duennebier 2002).

From relation (1), the mean pressure fluctuation, ΔP, induced by the waves at the sea surface, integrated over the range of depth $[0, H]$, will be:

$$\Delta P = \frac{1}{H}\int_0^H \frac{P_0}{\cosh(kh)}\, dh.$$

This integral can be evaluated exactly as follows:

$$\Delta P = \frac{P_0}{H}\left[\frac{2}{k}\arctan[\exp(kH)]\right]_0^H = \frac{2P_0}{kH}\left(\arctan[\exp(kH)] - \frac{\pi}{4}\right).$$

Substituting k by $2\pi/\lambda$, where λ is the wavelength, one obtains:

$$\Delta P = \frac{P_0\,\lambda}{\pi\, H}\left(\arctan\left[\exp\left(\frac{2\pi H}{\lambda}\right)\right] - \frac{\pi}{4}\right). \tag{2}$$

To calculate the maximum vertical ground displacement $W_{\max}$ induced by this pressure variation, we use the equation published by Kanamori (1989):

$$|W_{\max}|_Z = \frac{\Delta P\ \lambda}{4\pi\mu}, \quad \text{where } \mu \text{ is the basement shear modulus.} \tag{3}$$

Thus, substituting (2) in eq. (3), one obtains an expression for the average ground displacement excited by an average pressure field between depth 0 and H, along the shore slope:

$$|W_{\max}|_Z = \frac{P_0\,\lambda^2}{4\pi^2\,\mu\, H}\left(\arctan\left[\exp\left(\frac{2\pi H}{\lambda}\right)\right] - \frac{\pi}{4}\right). \tag{4}$$

In expression (4), P_0, is simply related to the swell height, h_s, via the well known hydrostatic pressure relation $P_o = \rho_w g h_s$, where ρ_w is the density of water, giving finally:

$$|W_{\max}|_Z = \frac{\rho_w g h s \lambda^2}{4\pi^2\,\mu\, H}\left(\arctan\left[\exp\left(\frac{2\pi H}{\lambda}\right)\right] - \frac{\pi}{4}\right). \tag{5}$$

Keeping in mind that we wish to obtain a rough estimation of the average ground displacement corresponding to a given oceanic swell, we have to set an appropriate range of values for μ and H. Concerning H, the depth of integration, it is accepted that the pressure fluctuation decays exponentially and becomes totally negligible at a depth of λ (Kibblewhite & Ewans 1985). Note also that the last factor ($\arctan[\exp(\frac{2\pi H}{\lambda})] - \frac{\pi}{4}$) has a very limited influence on numeric values, since it just varies within the limited range [0.21, 0.78] for H varying between 0 and infinity. A value of 0.74 is obtained for $H = \lambda$ and, inserting this in (5), one obtains the simple expression:

$$|W_{\max}|_Z = 0.74\ \frac{\rho_w\, g}{4\pi^2}\ \frac{hs\,\lambda}{\mu}. \tag{6}$$

Although the shear modulus for limestone and marble can be experimentally measured (e.g. Rasolofosaon *et al.* 1997), it can be expressed in terms of the mechanical properties of the sea floor, the velocity of P wave, α, and its density, ρ_s:

$$\mu = \frac{\rho_s\,\alpha^2}{3}, \text{ (assuming that rocks are Poisson's solids).}$$

Thus,

$$|W_{\max}|_Z = 0.74\ \frac{3\rho_w\, g}{4\pi^2}\ \frac{hs\,\lambda}{\rho_s\alpha^2} \tag{7}$$

Expression (7) can also be written as a function of the swell period, T, by substituting λ by $gT^2/(2\pi)$:

$$|W_{\max}|_Z = 0.74\ \frac{3\rho_w\, g^2}{8\pi^3}\ \frac{hs\,T^2}{\rho_s\alpha^2}. \tag{8}$$

It is important to note that the expressions (7) and (8) do not consider (i) any attenuation factor $A(\Delta)$ taking into account the distance between the bottom pressure field (source area) and the place where the ground displacement is measured and (ii) the directional properties $G(\theta)$ of the swell related to the shore orientation. For this second factor, the simplest form is $G(\theta) = \cos(\theta)$, with $\theta = 90^\circ$ for a swell approaching the shore perpendicularly. This model, based on simple static pressure considerations, should obviously overestimate the ground displacement. On the other hand, it predicts that $W_{\max}$ is dependent on the square of the swell period and is linearly related to the swell height. A more general formulation of the amplitude of the vertical ground motion could be the following:

$$|W_{\max}|_Z = 0.74 \ \frac{3\rho_w g^2}{8\pi^3} \ \frac{hs\,T^2}{\rho_s \alpha^2} \ A(\Delta)\, G(\theta). \qquad (9)$$

From seismic refraction experiments, Talandier & Okal (1987) determined values for the main parameters of the velocity structure of the carbonate cap of the Tuamotu plateau (3300 m s^{-1} for *P* wave velocity) and for the volcanic edifice of Tahiti ($Vp = 4370$ m s^{-1}). Taking a value of 2600 kg m^{-3} density for limestone and 3000 kg m^{-3} for basalt in expression (7) or (8), one should observe at the source (i.e. on the reef itself, with $A(\Delta) = 1$ and $G(\theta) = 1$) the maximum displacements summarized in Table 2, for swells of various periods and for significant height $h_s = 1$ m which is a typical value.

Since the horizontal noise along the major axis is generally 3 to 5 times larger than the vertical noise (as illustrated Figs 2 and 4), the magnitude of the horizontal SF microseismic noise induced by a 1-m-high swell is, therefore, expected to vary in the range 6–30 μm. As shown in Figs 4(c) and 5, the microseismic background noise amplitude in the SF band observed on the Polynesian atolls is generally smaller, between 1 and 2 μm. On 2003 January 20, for instance, the noise amplitude observed at MAT and TAK (Figs 5a and b) is about 2 μm, that is, of the same order of magnitude as the calculated vertical ground motion. During swell episodes, the noise amplitude at those stations reaches 10 to 20 μm.

On volcanic islands such as Tahiti, where stations are installed at larger distances from the shore (a few kilometres), the recorded SF noise amplitude is clearly smaller. This characteristic was already evident from the PSD analyses. As shown Fig. 5(c) and also discussed below, the background noise at PPTL is typically of the order of 0.2 to 0.4 μm; the swell-related peak reaches 2.0 to 3.0 μm but never exceeds these values. We suggest that this overall smaller amplitude of microseismic noise variation must be related to the larger distance of the sensor from the reef and could indicate a signal attenuation and/or a geometric spreading, plus the effect of the angle of the incoming swell relative to the exposed shore orientation. Consequently, the relations (7) and (8) would be valid for stations very close to the exposed reef and receiving swell perpendicularly to the barrier. For inland stations at several km from the coast such as PPTL, the attenuation factor $A(\Delta)$, which decreases with the distance Δ from the shore cannot be ignored.

Table 2. Maximum vertical displacement, $W_{\max}$, in microns, calculated from expression (8), as a function of the swell period T and wavelength λ, for a significant height $h_s = 1$ m, for atolls ($W_{\max} = 3.0 \times 10^{-8}\, h_s\, T^2$) and volcanic islands ($W_{\max} = 1.5 \times 10^{-8}\, h_s\, T^2$), taking appropriate values of the parameters ρ_s and α.

Swell period T (s)	8	10	12	14	16	18	20
Swell wavelength λ (m)	100	150	225	300	400	506	624
$W_{\max}$ for atoll (μm)	1.9	3.0	4.3	5.9	7.7	9.7	12.0
$W_{\max}$ for volcanic island (μm)	0.9	1.5	2.2	2.9	3.4	4.9	6.0

From the above simple calculations and the noise amplitude results, $A(\Delta)$ should be close to 0.5 at the atoll stations and 0.2 for PPTL, which is 3 to 4 km distant from the reef. We emphasize that this attenuation only concerns the SF peak, and is fundamentally different from that for the DF peak. If the signal corresponding to the DF peak is able to propagate as Rayleigh waves over a very long distance (e.g. Bromirski *et al.* 1999; Schulte-Pelkum *et al.* 2004), the attenuation of SF peak is very strong even at short distances, as shown in Fig. 6.

Consequently, inserting the appropriate values of $A(\Delta)$, eq. (8) takes the following simple forms:

$|W_{\max}| = 1.5\ 10^{-8}\ T^2\ h_s$, for atoll islands and

$|W_{\max}| = 0.3\ 10^{-8}\ T^2\ h_s$, for PPTL station (Tahiti),

where T is the swell period in seconds and h_s the significant wave height in metres. $|W_{\max}|$ will be in metres.

4.2 Microseismic noise correlation between islands

We present in Fig. 5 the SRSN amplitude measured each hour during the month of 2003 January at stations MAT, TAK and PPTL. Although MAT and TAK (installed in the northern Tuamotu) are 400 km apart, the similarity of their SF noise patterns is striking: the individual peaks arrive at similar times and the noise amplitudes at the two stations, located at similar distances from the reef, are approximately the same. The SF noise observed at MAT and that observed at TAK are strongly correlated, with a correlation coefficient R of 0.83.

For the period 2002 August–September, the SRSN variations for most stations are similar. The examples presented in Fig. 7 are for stations ANA and REA. Both atolls are in the Tuamotu archipelago, separated by about 1000 km. The correlation between the SRSN variations at the two sites is obvious. The linear fit between the SRSN amplitudes measured at these two sites has a high correlation coefficient ($R = 0.84$). There are, however, some differences in the amplitudes. If the background noise is of the order of 2 microns at both sites, the SRSN amplitude at REA is almost twice that observed at ANA for most swell peaks. For instance, the September 4 swell peak induced a ground motion of 25 μm at REA but only 15 μm at ANA. This results in a value of the slope of the linear fit close to 0.5. The different behaviour of the two stations could be related to the site distance from the reef, and therefore, to the factor $A(\Delta)$ in eq. (8). Reao and Anaa atolls are both NW–SE elongated atolls (elongation ratio, respectively, 1:6 and 1:7) and in both cases the seismic stations are installed close to the northern shores. The main geometric difference is that Anaa atoll is more than 5 km wide while Reao is less than 2 km wide, implying that the noise source for southerly swells (i.e. the external slopes of the southern reef) is much closer to station REA than ANA.

The high signal correlation in the frequency range 0.05–0.077 Hz between seismic stations separated by several hundreds of kilometres could appear as contradictory when considered with the fact that the amplitude of the SF peak is strongly attenuated as the distance from the reef increases. Both observations can be easily reconciled if the signal has a remote origin, much larger than the distance between stations, and produces a large-scale effect. The swells generated by oceanic storms are good candidates for a remote source since they have a very distant origin (the northern Pacific ocean during the boreal winter and the southern Pacific during the austral winter). These remote storms generate waves in the SF frequency

range, which travel through the whole Pacific Ocean and interact locally with the reefs, roughly simultaneously at the various islands (depending on their location relative to the swell front) to generate the observed SRSN.

4.3 Comparison of the SRSN with the NOAA wave predictions

An operational, seven-day swell forecast is provided by the NOAA Ocean modelling group. Ocean wave development, dissipation and propagation through the various oceans are calculated by the finite difference model NWW3 (NOAA WaveWatch III) algorithm. The only driving force considered in this model is the wind field. Wave spectra are calculated at each node of a 1.25° longitude by 1° latitude area. The wave height as a function of the wave frequency is given for 24 azimuths (Booij & Holthuijsen 1987; Tolman & Chalikov 1996; Booij *et al.* 1999).

The spatial resolution of the model is of the order of 100 km, somewhat less than the typical distance between stations. However, it is particularly important to note that the French Polynesian islands are not taken into account in the model, although they may play an important role locally in dissipating the swell energy along their shore lines. This limitation was pointed out by Tolman (2001) to explain discrepancies between the predicted and the remotely observed swell amplitudes (from the ERS-2 satellite) in French Polynesia. As shown below, some of the differences between our observed SRSN and the predicted wave height may be due to this model limitation. In particular, we show in Section 4.6 that the alignment of the atolls of the Tuamotu archipelago creates a natural barrier to the swell whose effect is visible in our seismic noise measurements.

Since the use of the full wave spectrum at each node of the model and for each time interval would take too much computer time, the full spectra are considered only at particular locations. Only the significant wave height *Hs* (corresponding to the average of the highest one-third of the waves), wave azimuth, *Dp*, and peak wave period, *Tp*, are kept at each node of the model, at three hourly intervals.

To compare the SRSN measured on the Polynesian islands with the NOAA predicted swell, we extract *Hs*, *Dp* and *Tp* at the nearest nodes of the grid to our seismic stations from the 'NWW3' global data set. These nodes are always less than 50 km from the nearest seismic station. This distance of the stations from the nodes will not noticeably affect the comparison between the wave model and the seismic noise because there is generally no strong short scale variation (<50 km) of the swell parameters. The measured SF noise magnitude and azimuth are, therefore, directly compared to the values *Hs* and *Dp* calculated at the nearest model node. It should be noted that *Tp* is the dominant wave frequency and does not exclude the possibility of the occurrence of swell events of higher frequency than the ones we measure.

When comparing measured SF noise with swell predictions, it is important to keep in mind some model limitations. First, the full complexity of the wave spectrum at a given site is not taken into account. This means, for instance, that the presence of several swells of different azimuths, which is a rather common occurrence (example shown in Fig. 3), is not taken into account and, therefore, can be a source of discrepancies. Secondly, if the frequency of the dominant wave height is higher than our maximum considered frequency of 0.077 Hz, the comparison is not valid.

To illustrate the discrepancies which can be induced by high frequency (<10 s) swells, we present in Fig. 8 the variations of the observed noise amplitude (the dots with a continuous line fit), together with the predicted *Hs* (dashed line) at TAK on Takaroa atoll in 2003 January. On Fig. 8(a), the overall correlation between the noise amplitude and *Hs* is good for the maxima but some discrepancies between the two curves are present, as for instance between January 18 and 22. The variations of the swell peak period with time predicted at TAK for 2003 January (Fig. 8b) clearly display the successive swell events affecting this atoll. Each event is 2–8 days long and is generally characterized by a continuous decrease in the wave period, long period waves travelling faster than short period waves. It is particularly clear in Fig. 8(b) that the period of discrepancies, January 18 to 22 corresponds to the occurrence of waves with periods shorter than 13 s. Waves of these periods have been rejected by filtering from our measurements. If we limit the period range of the predicted swell to 13–20 s (our measurement window), the correlation with the observed microseismic noise (Fig. 8c), is much better although differences in amplitudes are apparent. This example indicates that the parameter *Tp* has to be carefully considered together with *Hs*. We discuss this further in the next section.

4.4 Correlation between the SRSN amplitude and the swell height—influence of the swell period

At each seismic station, the swell-related signal amplitude is obtained each hour by measuring the length of the horizontal ground elliptical motion. We present in Fig. 9 the variations of this observed noise amplitude at MAT and REA for 2002 August–September (Figs 9a and c) and 2003 January (Figs 9b and d). A systematic feature visible in Fig. 9 is the good correlation between the observed microseismic noise peaks and the predicted swell peaks. As already noted for TAK (Fig. 8), each peak of the wave height represents a swell front and corresponds to a peak in the seismic noise amplitude. The snapshots of the WaveWatch model output present the variations of the peak wave period parameter *Tp*, and illustrate the arrival of two particular swell fronts in French Polynesia, on 2002 September 4 (Fig. 9e) and on 2003 January 13, (Fig. 9f), arriving from the south and north, respectively. The swell front is characterized by the longest swell periods, which are in the range 18–20 s for these particular examples.

Low noise episodes correspond to periods of low swell heights, which are generally of period shorter than 13 s, and are not plotted in Fig. 9. The correlation of the observed noise amplitude with the predicted *Hs* strongly depends on the overall site quality, that is, on the amplitude of the mean noise level in the considered frequency band. If the fit is particularly good at some stations such as MAT, REA, TAK, HAO and ANA, that is, all the stations in the Tuamotu, it is of much lower quality at stations such as RAP and RUR, probably due to the fact that the data from these sites are of lower quality in the SF band. Similarly, despite the fact that the Marquesas station HIV is of rather high overall quality (see PSD in Fig. 2a), it appears to be of poor quality with respect to the swell-related noise. Station HIV is installed on a volcanic island a few km from the shore and the low SRSN level could be caused by signal attenuation. Interestingly, the latter three islands also have no lagoon. Their shore geometries are more complex and the bathymetries are known to be steeply sloping. These factors could possibly inhibit the transfer of energy between the swell and the island.

A more detailed analysis of the correlations between the seismic noise amplitude and the significant swell height *Hs* shows some amplitude discrepancies. For instance, the swell fronts were expected to have similar amplitude on 2002

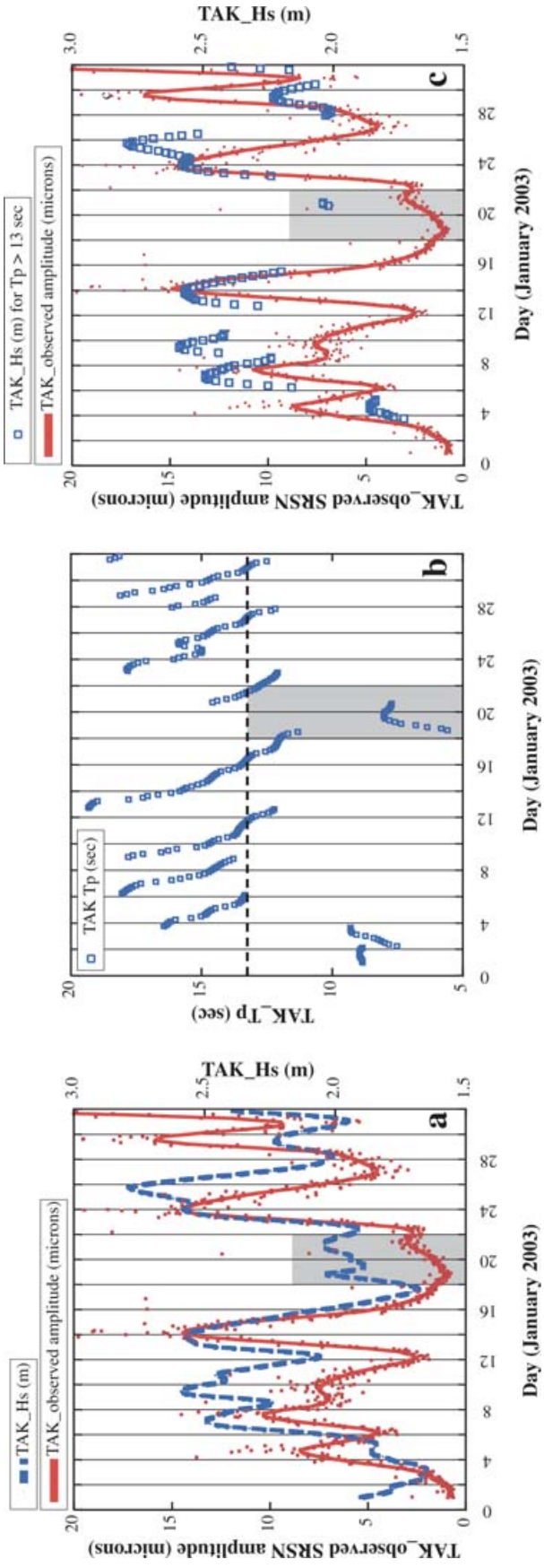

Figure 8. Comparison of the noise amplitude measured at TAK in 2003 January with the predicted swell height *Hs* derived from the NOAA NWW3 model. (a) The seismic noise measurements are presented as red dots with a smoothing curve (continuous red line). Superimposed is a dashed blue line corresponding to the variations of the predicted *Hs* at that location. The overall agreement between the measured and predicted peaks is fair, but some discrepancies are visible (for instance in the shaded area). (b) Variations in the predicted peak wave frequency (parameter *Tp*) during the same period to illustrate the occurrence of periods of swell of high frequency. Note that the shaded area between January 18 and 22 corresponds to high frequency swell. (c) Noise measurements (red dots) and predicted *Hs* (blue squares) restricted to the long period swells ($Tp > 13$ s).

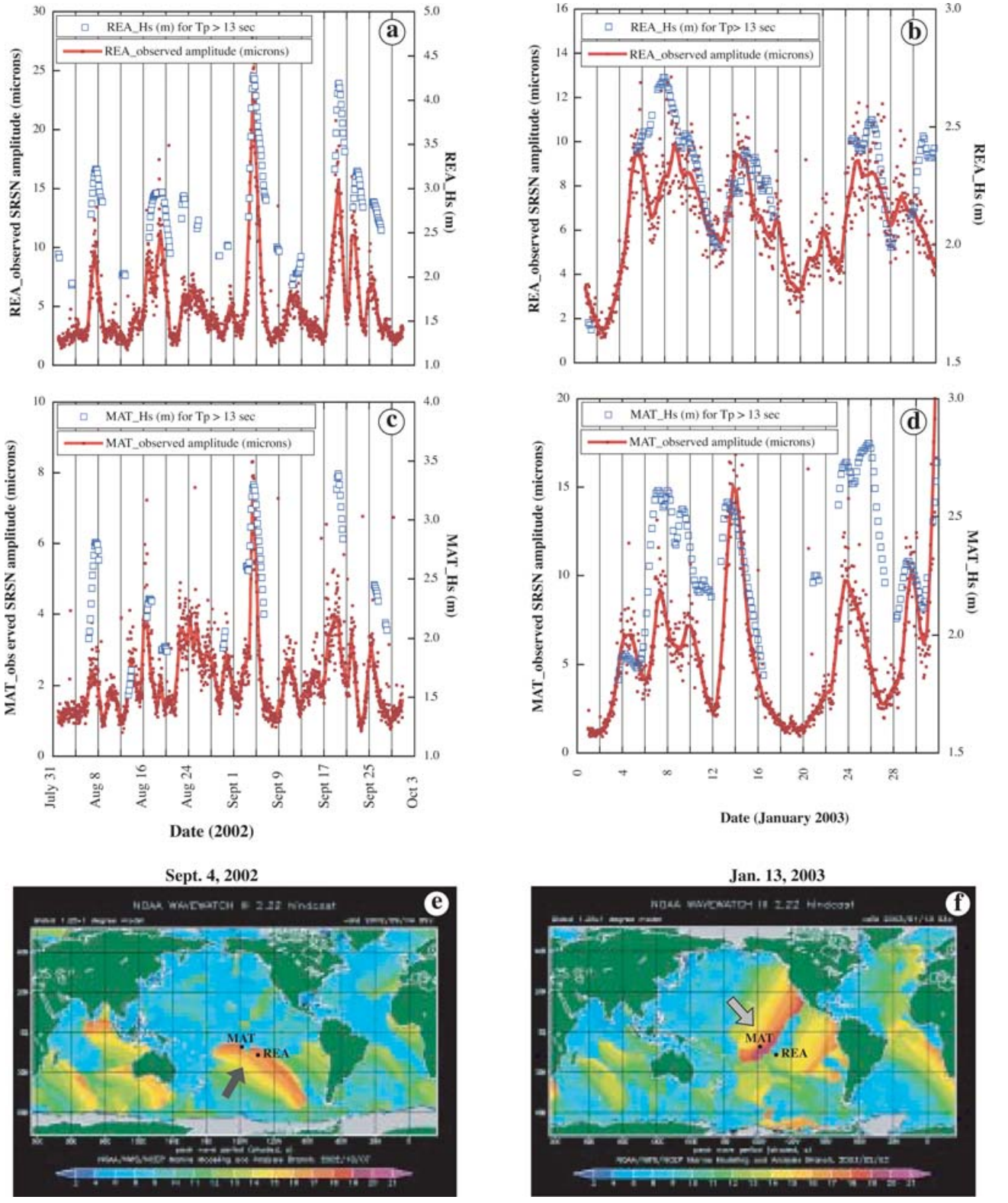

Figure 9. Comparison of the hourly values of seismic noise (red dots, in microns) with predicted amplitudes *Hs* (blue squares, in metres) for *Tp* > 13 s at REA (a and b) and MAT (c and d) for the two periods 2002 August–September (left) 2003 and January (right). Correlations between the peaks are clear although some amplitude discrepancies are observed at MAT. This figure illustrates that the swell-related microseismic signal may be used as a proxy for the swell amplitude. In (e) and (f) are presented snapshots of the NWW3 model output of the swell peak period *Hs* for 2002 September 4 (e) and 2003 January 13 (f). The location of MAT and REA is indicated on these maps. These two examples illustrate the arrival of swell fronts with, respectively, a southern and a northern component that are clearly visible in the seismic measurements. The arrows show dominant directions. Note that swell fronts from the south arrive at roughly the same time at the two stations (e.g. on September 4) as expected from the model, whereas the northern swell arrives earlier at MAT (e.g. on January 14) than at REA (January 15).

September 5, and on 2002 September 19, at stations MAT and REA (Figs 9a and c). The actual swell-related signal amplitudes at both sites are a factor of two lower for the September 19 event than for the September 5 event. Since both events arrived from the SW, such a difference is not well understood but could correspond to the attenuation factor $A(\Delta)$ described above.

The propagation time of the swell front between the two stations is also visible on Fig. 9. The SW incoming swells are expected to reach MAT and REA roughly simultaneously, as on September 4 for instance (Fig. 9e), which is what is observed in the SRSN measurements. Conversely, for the NW incoming swell, one should expect there to be some difference in its arrival time at the two stations. For the MAT January 13 event for instance, the maximum amplitude is visible at the end of January 13. This event occurs in the middle of January 14 at REA.

In order to quantify the influence of the swell period on the SRSN amplitude, we plot in Fig. 10 the SRSN recorded at station REA during the months of 2002 August–September and 2003 January as a function of the NOAA-predicted swell height *Hs*. To produce Fig. 10 we filtered and processed the same data set as that presented in Figs 9(a) and (b) successively in two frequency windows: first between 11 and 14 s (0.091–0.071 Hz, open squares) and then between 14 and 20 s (0.071–0.05 Hz, filled circles). Also plotted in Fig. 10 are the values of $W_{\max} = 1.5\,10^{-8}\,Hs\,T^2$ from eq. (8), which correspond to the theoretical variations of the SRSN for some selected swell periods (8, 10, 12, 14, 16, 18 and 20 s). Fig. 10 shows several interesting features: (i) for a given predicted swell height, long-period swells generate a stronger SRSN. (ii) Data filtered in the 11–14 s period are well grouped between the 8 and 14 s lines calculated from eq. (8). (iii) Although data filtered in the 14–20 s are spread between the 8 and 18 s theoretical lines, the domain between the 16 and 20 s theoretical lines is clearly restricted to long period signals. This diagram, therefore, suggests that the noise amplitude in the SF peak is primarily associated with the longest swell periods.

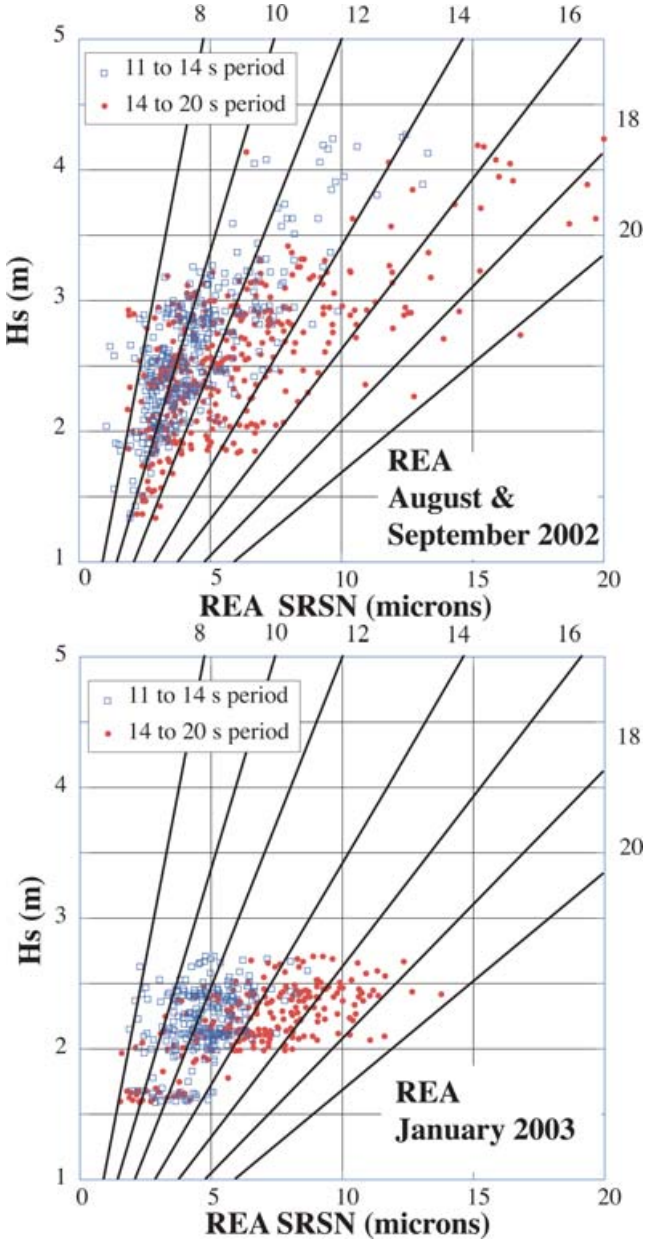

Figure 10. Swell-related seismic noise recorded at station REA in the Tuamotu in 2002 August and September (left) and in 2003 January (right) as a function of the predicted swell height *Hs* for two period ranges: 11–14 s (blue squares) and 14 to 20 s (red dots). Also plotted are the relations calculated from eq. (6) for periods between 8 and 20 s.

4.5 Analysis of polarization at the permanent PPTL station for the whole year 2003

The amplitude of the ground displacement is related to the swell height through a transfer function (e.g. Bromirski *et al.* 1999). This transfer function depends on the site distance from the shore, and on other parameters which link the pressure variations generated by the swell along the reef slope to the actual seismic noise. These parameters are likely to include the degree and nature of the coupling with the hard rock, and the shore geometry. We have made a complete and continuous SRSN analysis for the permanent LDG/CEA seismic station PPTL installed in Tahiti for the whole year 2003. The aim of this analysis is to complement on a long-term basis the short-term tests performed on a few months of data recorded by temporary PLUME seismic stations. As already demonstrated by Bromirski *et al.* (1999) for seismic station BKS located on the United State west coast, or by Grevemeyer *et al.* (2000) for station HAM running in Germany, seismic stations that have been running for decades provide seismic archives that may be used to analyse the long-term variations of swells and, therefore, to investigate indirectly climate changes. In French Polynesia, PPTL is the most appropriate instrument for such a purpose since it is a high quality permanent station and since it has run for several decades and is still running. Its ability to produce routine values of the swell height and azimuth will, therefore, be discussed.

A noise polarization analysis was performed on PPTL data over the entire year 2003 by processing each hour the continuous recording of the three long period components. PCA is performed after filtering the signal in the [0.05–0.075] band. Most of the approximately 2300 earthquakes recorded each year at PPTL are automatically rejected from the results. This is done (i) by rejecting signals having incident angle less than 80°, (ii) by ignoring peak to peak perturbations larger than 5.0 microns, (iii) by retaining only those signals having *CpZ* (vertical polarization coefficient) greater than 0.80, and (iv) by retaining only those signals with *CpH* (horizontal polarization coefficient) greater than 0.65.

The results of the noise polarization analysis are presented in Fig. 11. For clarity, the results are plotted in two parts, each covering a six-month period. The NOAA predicted swell height (right vertical axes) clearly shows several large swell episodes over the

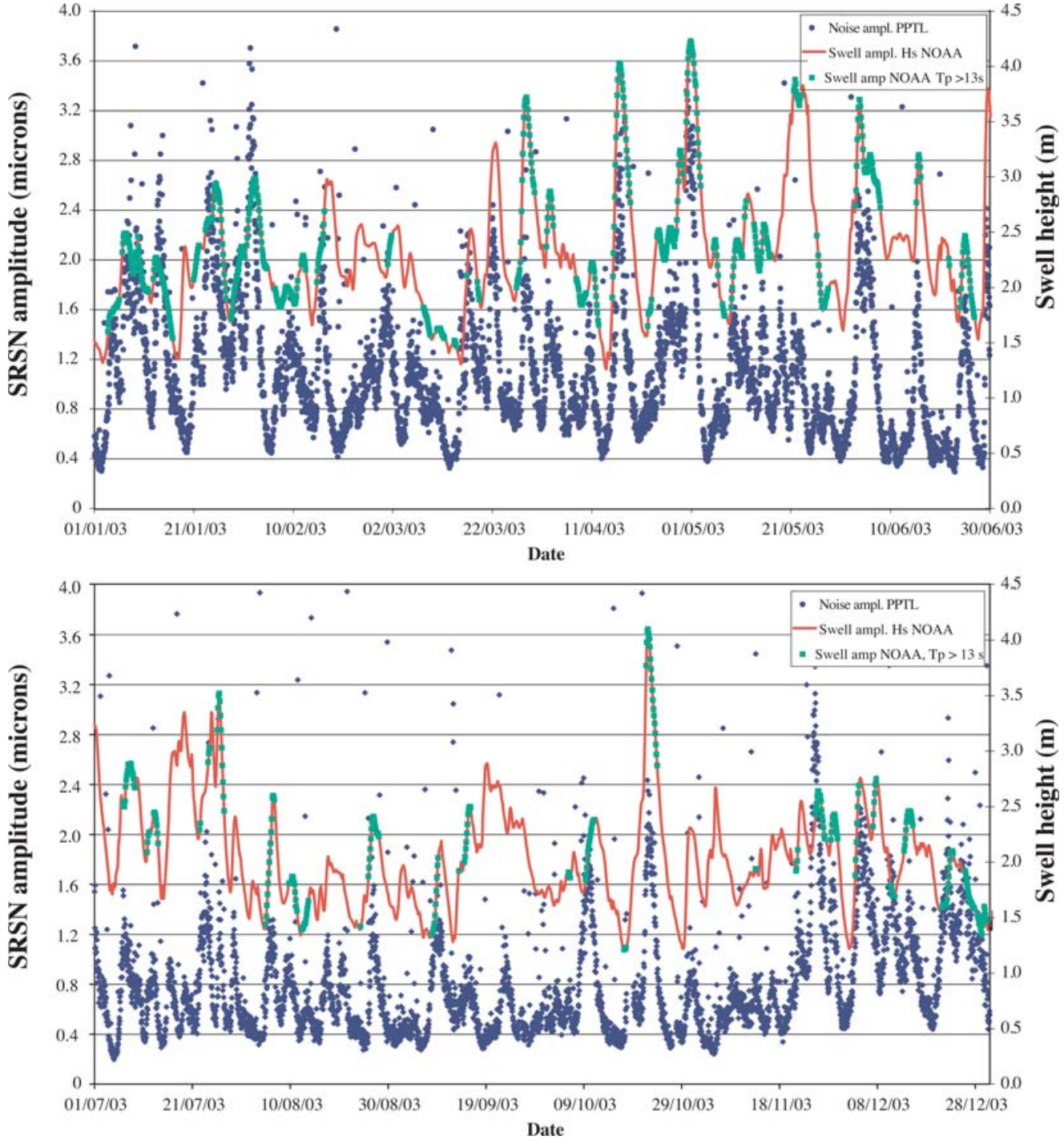

Figure 11. Hourly amplitudes of swell-related seismic noise (blue dots, in microns) recorded at PPTL on Tahiti island for the whole year 2003. (a) 2003 January to June and (b) 2003 July to December. Also plotted are the NOAA-predicted swell amplitudes *Hs* (continuous red line). The swells of periods greater than 13 s are distinguished by green squares on the amplitude curve.

year. The long period seismic noise (left vertical axes) generally shows the same trends as the swell height, with the best correlations corresponding to the large peaks of noise induced by the largest swell episodes.

After separating data corresponding to the southern and northern incoming swells (on simple criteria based on date and on measured swell azimuth), we determine (Fig. 12) the 'transfer function' linking the NOAA predicted swell heights *Hs* to the observed microseismic amplitudes *A*. As shown below, Tahiti island is clearly not excited in the same way by the different swells.

The best fit through the data appears to be a log relation of the form:

$Hs = 1.18 \ln(1000\,A) - 4.80$ for the southerly swells (Fig. 12a), and

$Hs = 0.468 \ln(1000\,A) - 0.86$ for the northerly swells (Fig. 12b)

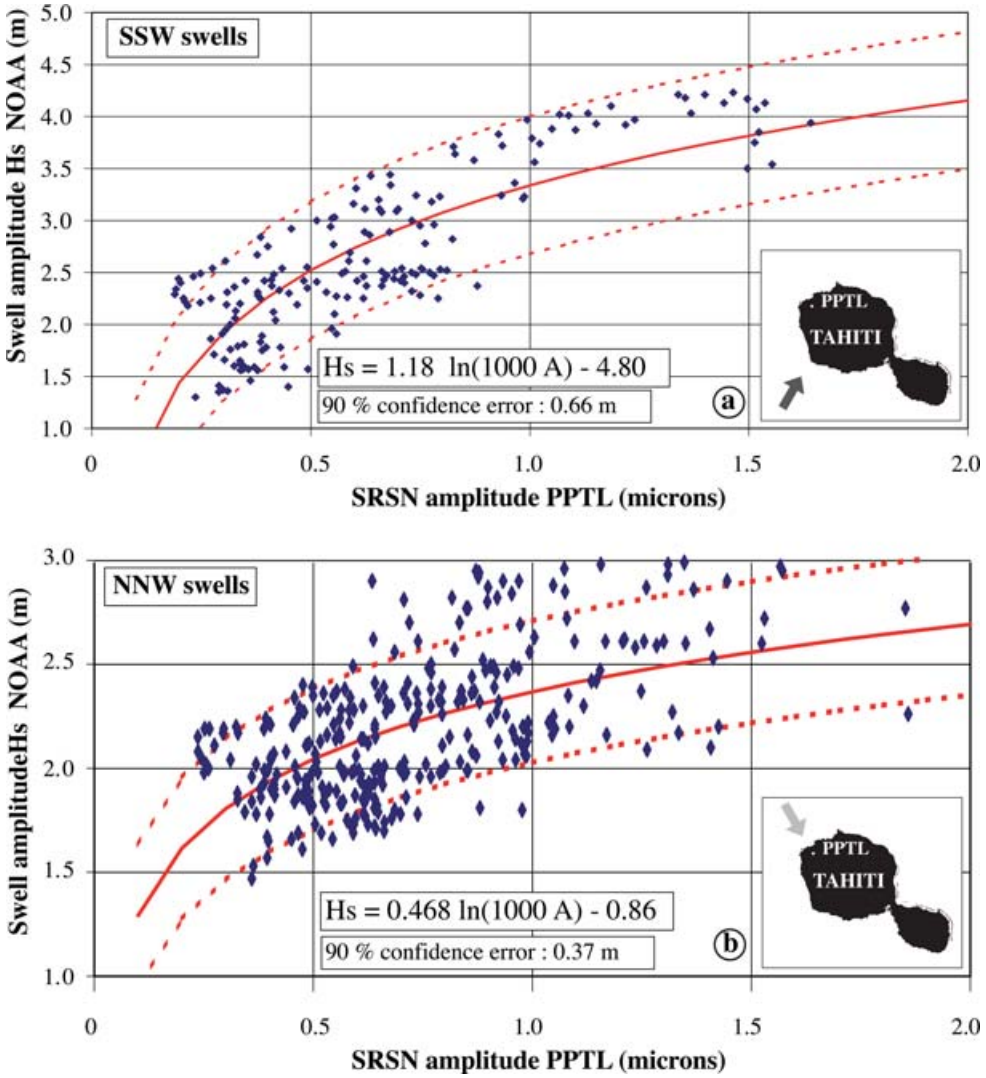

Figure 12. Transfer functions relating the predicted swell amplitudes (in m) to the observed microseismic noise amplitude (in microns) at station PPTL on Tahiti island. Northerly (a) and southerly (b) swells have been separated. Northerly swells clearly excite the island more efficiently than southerly swells. In other words, a swell of a given height generates a larger seismic signal when it arrives from the north than when it reaches Tahiti from the south. Note that the 90 per cent confidence error is rather small in both cases (0.66 and 0.37 m respectively) and indicates that the seismic noise amplitude is a good proxy for the swell height.

Hs is the swell amplitude in metres and *A* is the observed seismic noise amplitude in micrometers along the principal polarization direction.

The aim of such transfer functions is to deduce a swell height from the SRSN amplitude. Occasional wave heights appear to be overestimated by the NOAA forecasting. On 2003 October 19, for instance, the seismic noise recorded at PPTL should correspond to a 3.0 m high swell rather than to a 4.0-m-high swell as predicted. On the other hand, some swell heights seem to be underestimated by the NWW3 prediction. The noise peak occurring at the end of 2003 November should correspond to a swell about 4.0 m high whereas only a 2.0- to 2.5-m-high swell was predicted by NWW3.

The two transfer functions are notably different: they show that for a given swell height, the northerly swells will generate a larger seismic signal than the southerly swells. This result may be associated with the fact that the swell periods are generally longer for northerly swells than for southerly ones. However, it could also be due to the attenuation of high frequencies with propagation, or it could be a consequence of the shape of the island and of the location of the seismic station on the northern side of Tahiti island. We have already shown above that the SRSN amplitude appears to be strongly dependent on the distance from the active reef, which may explain the difference here.

Despite these occasional discrepancies, it is interesting to note that the 90 per cent confidence errors are low, with values of only 0.37 m for northerly swells, and 0.66 m for southerly swells. These values are small enough to provide a precise estimation of the swell height from the microseismic noise amplitude. This is of particular importance for French Polynesia where buoys are not available for direct measurements.

4.6 The Tuamotu: a barrier to the swell

The Tuamotu seismic stations are of good quality and most of them display good correlations between the recorded noise amplitude and the predicted wave heights. Two of them, however, (ANA and TAK)

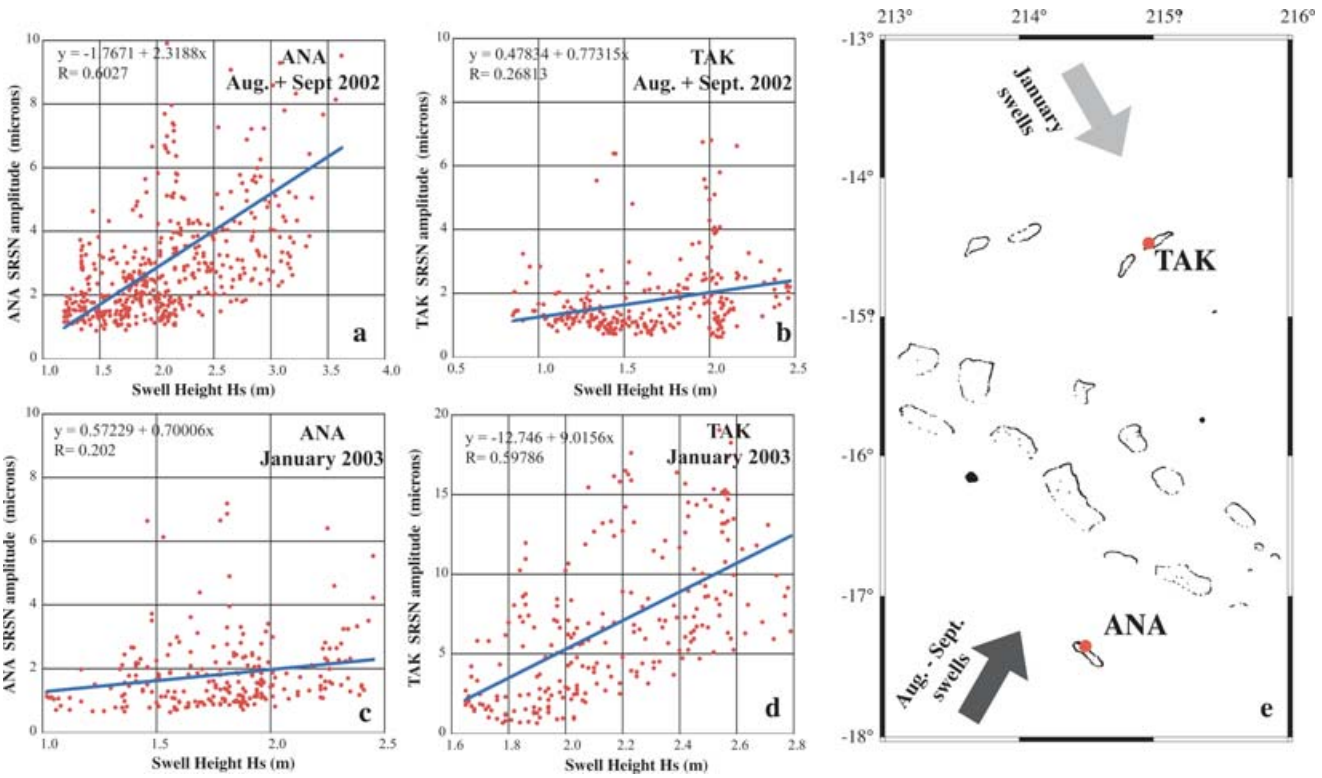

Figure 13. Seasonal variations of the swell-related seismic noise at ANA and TAK in the Tuamotu. During the austral winter (August and September), the noise amplitude measured at ANA (a) shows strong variations reasonably well correlated with *Hs* (the linear fit has a coefficient $R = 0.60$) whereas the same swell appears to have little effect at TAK (b), where the correlation with *Hs* is small ($R = 0.27$). The opposite behaviour is observed during the austral summer (January), when swell arrives from the North: TAK (d) has large noise amplitudes, well correlated with *Hs* ($R = 0.60$), whereas ANA (c) has weak noise variations poorly correlated with *Hs* ($R = 0.20$). The continuous geographical alignment of the atolls between the two stations ANA and TAK (e) may prevent the swell from travelling freely across this part of the Tuamotu. ANA, therefore, appears to be protected from North-coming swell by the barrier (during boreal winter) whereas TAK could be protected from southerly swell events (during the austral winter).

have an apparent seasonal behaviour in their transfer functions. Depending on whether the swells arrive from the North or from the South, their responses differ noticeably. Interestingly, these two stations are roughly at the same longitude, at slightly more than 300 km from each other, but are separated by a zone of high concentration of atolls (see Fig. 13e).

In 2002 August–September, during the austral winter, when swells arrive from the South, ANA, on Anaa atoll, on the southern side of the Tuamotu, has swell-related noise amplitude variations in the range 1–10 microns (see Fig. 13a). During the same period, TAK (Fig. 13b), on Takaroa atoll, on the northern side of the Tuamotu, has amplitudes generally smaller than 4 microns. During this period, the slope of the transfer function is, therefore, very different at the two stations, and there is a much better correlation between the swell height and the SF microseismic noise amplitude at ANA than at TAK. The linear fit between the ground displacement and the predicted *Hs* gives a small correlation coefficient at TAK ($R = 0.27$) and much higher one at ANA ($R = 0.60$).

In 2003 January, during the boreal winter, we observe the opposite behaviour between ANA and TAK. Despite a swell height lower than 3 m, TAK has a SF microseismic noise amplitudes in the range 1–20 microns (Fig. 13d), whereas those at ANA (Fig. 13c) vary little and are generally in the range 1–4 microns. The slopes of the transfer functions are inverted relative to those of the summer period. The resulting correlation between the ground displacement and the predicted *Hs* is high at TAK ($R = 0.60$) and low at ANA ($R = 0.20$).

This seasonal behaviour cannot be explained by the signal attenuation within the island since ANA and TAK stations are both situated on the northern rim of the Anaa and Takaroa atolls. The atolls also have a similar shape. A map of the northern Tuamotu (Fig. 13e) shows that between the atolls of Takaroa and Anaa, the archipelago is composed of two alignments of atolls in the NW–SE direction, some of them being among the longest in the world (e.g. Fakarava, more than 50 km long). Swells cannot propagate freely across this area since the swell energy would be strongly reflected and diffracted by the atolls. The transmitted amplitude would be strongly attenuated after the crossing of this part of the Tuamotu. Thus the local geometry of the Tuamotu archipelago may explain the apparent 'seasonal' behaviour of these two sites, with a low swell-related noise and hence a poor correlation between the noise and *Hs* at the station protected by the barrier and the opposite at the station in front of the barrier. More generally, the high concentration of atolls may also explain in some particular cases the differences between the swell height in the southern-central Pacific (predicted by a model which does not take into account the islands bathymetry) and the swell height deduced from the observed SRSN. Our ground measurement analysis supports the conclusions of Tolman (2001) with regard to discrepancies between the predicted swell heights and the swell amplitudes deduced from ERS-2 satellite altimetry.

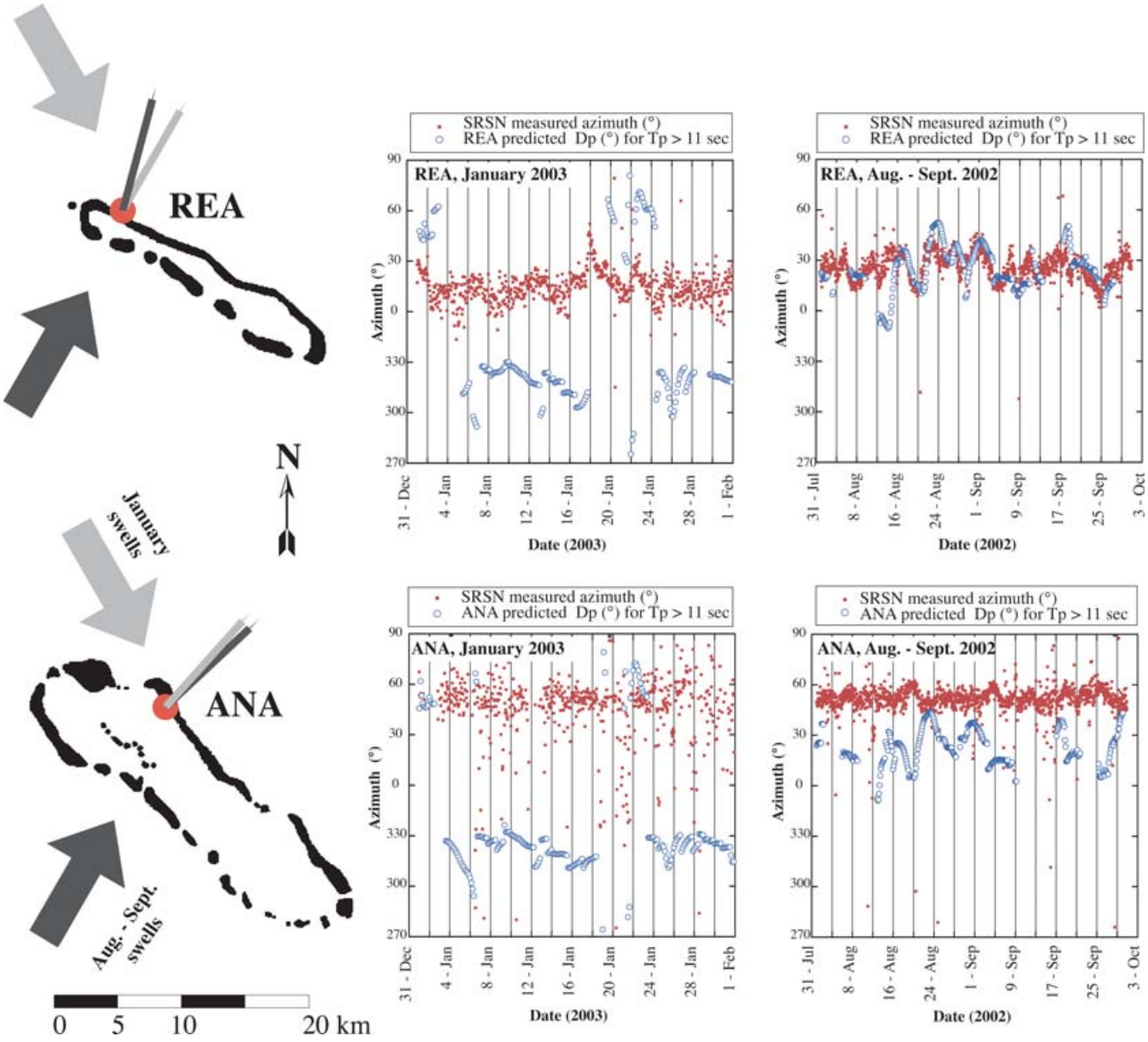

Figure 14. Comparison of the observed noise azimuth with the NWW3-predicted swell direction *Dp* at four Tuamotu stations. (a) REA and ANA; (b) MAT and TAK. For each station, we present the swell-related seismic noise azimuth for the two selected periods (winter and summer, i.e. for southerly and northerly swells). The red dots represent the hourly values of the azimuth of the ground motion (for the period range 13–20 s) and the blue circles represent the NWW3-predicted swell azimuth *Dp* for swell periods greater than 11 s. Note that the azimuths of ground vibrations recorded at elongated atolls show weak variations and appear to be 'locked' around the direction normal to the atoll long axis. Only at MAT (on an almost circular atoll) is there a good correlation between the recorded noise azimuth and *Dp*. On the left-hand side are maps of the different atolls at the same scale, with the incoming swell direction indicated by the thick arrows (black for southerly and grey for northerly) and the mean direction of measured microseismic noise azimuth indicated by the straight lines with the same color code as the arrows. Note that the swell excitation direction and the corresponding island response for the two seasons are approximately parallel only at MAT. At the other stations, the ground response is normal to the atoll long axis and may be, therefore, oriented at a large angle from the swell direction. This illustrates the effect of wave refraction which tends to make the swell wave fronts parallel to the shoreline.

5 QUANTIFICATION OF SWELL AZIMUTH FROM MICROSEISMIC NOISE

5.1 SRSN azimuth and swell direction correlation

The azimuth of the ground elliptical motion was measured each hour at the PLUME and LDG stations for the summer and winter periods considered in Section 4 above. The primary aim in selecting two periods during the austral and boreal winter was to test the ability of the seismic noise to detect reliably the azimuths of the incoming swell. We present in Fig. 14 the azimuthal variations during these two periods (red dots), for four PLUME stations (REA, ANA, TAK and MAT), with for comparison the NWW3-predicted swell directions *Dp* (open circles).

During the austral winter, swells are generated mostly in the South Pacific and cross French Polynesia broadly from the SW (see example of swell front in Fig. 9e). For the selected period, 2002 August to

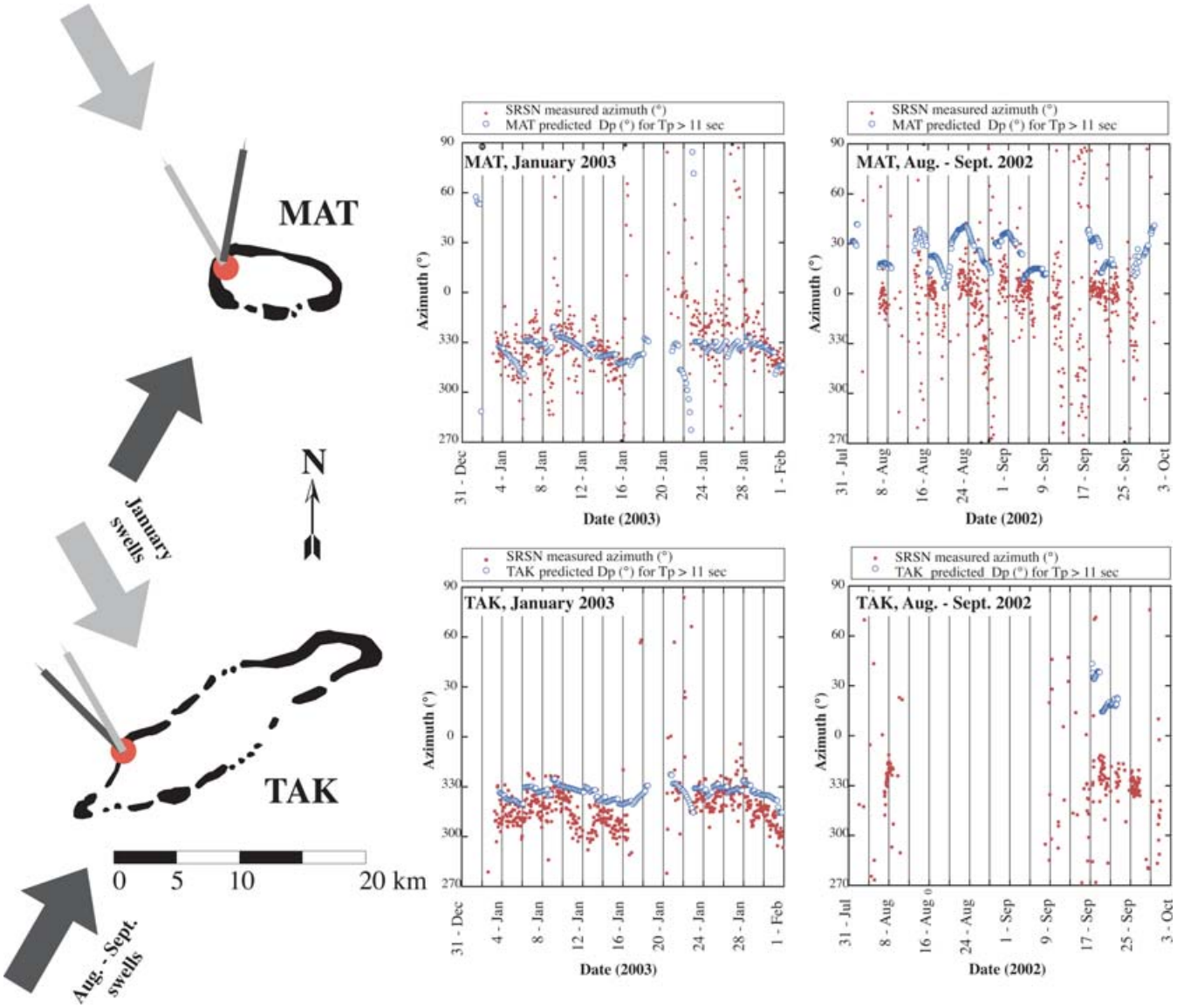

Figure 14. (*Continued.)*

September (Fig. 14), the predicted swells propagate with azimuths between 20° and 50° (which corresponds to 200° to 230° with a 180° ambiguity). During the boreal winter (January), long swells are generated in the northern Pacific and cross French Polynesia with NW to NNW azimuths (example in Fig. 9f). In 2003 January, most of the swells arrive from azimuths in the range 310° to 330° (Fig. 14).

Of the four stations presented in Fig. 14, only MAT shows a good fit of the measured noise azimuth (dots) with the predicted *Dp* (open circles), for both the SW and NW incoming swell azimuths. It can be noted, however, that the fit is much better in January than in August and September. Indeed, in January, the quality of the fit reveals second order variations such as small rotations of the swell azimuths within a given swell event. Such a feature can be seen in our data, for instance between January 3 and 6, when there is a small counter-clockwise rotation of the seismic noise azimuth apparently well correlated with the predicted swell azimuth rotation.

Stations REA, ANA and TAK are characterized by the fact that the azimuth of the seismic noise in the period range 13–20 s appears to be fixed, whatever the azimuth of the incoming swell. The fit between the observed and the predicted azimuth at REA is very good (both oscillating between 20° and 30°) during the austral winter (particularly between August 16 and September 4: see Fig. 14a), but very poor in January since the observed azimuth remains between 10° and 30° while the swell fronts arrive mostly from the NW. Similarly, the noise azimuth at TAK shows a good fit with the azimuth of the northerly swells (January) but not with southerly events (August–September). Ground vibrations at ANA appear to be imperturbably 'locked' around 50°, whatever the azimuth of the incoming swell.

5.2 Swell refraction and atolls anisometry

The origin of the particular behaviour of the horizontal particle motion observed at ANA, TAK and REA may reside in the highly anisometric geometry of the atolls on which they are installed, respectively at Anaa, Takaroa and Reao. All these atolls are elliptical in shape (see Fig. 14) and have a large aspect ratio (about 1:6 for

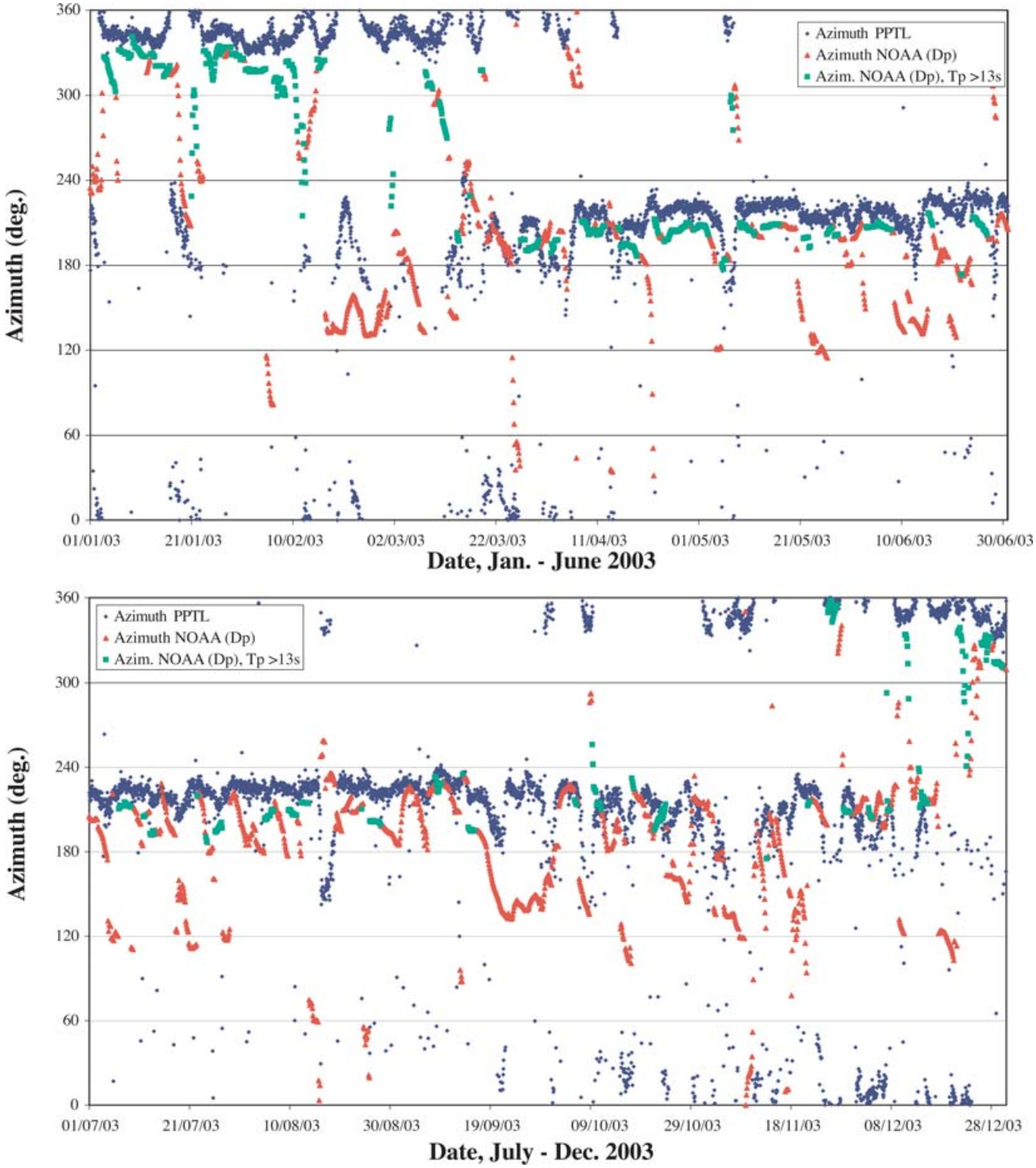

Figure 15. Swell-related seismic noise azimuth recorded at PPTL on Tahiti island for the whole year 2003. (a) 2003 January to June and (b) 2003 July to December. The hourly observations are represented by blue dots and the NOAA-predicted swell azimuths *Dp* by the green squares for swells of periods greater than 13 s and by the red triangles for higher frequency swells. Note that the observed azimuths follow the same trends as the predicted ones (NOAA, *Dp*), with a systematic deviation of about 10° (not yet explained). Globally, the southerly swells start in April, while the northerly swells are ending at this time. The direction of the southerly swells is constant over the year (azimuths of 220–240°). Some discrepancies between the measured azimuth and the NWW3 model are clearly observed in February: the observed azimuth is SW while the predicted is SE. In March, we deduce a long period N swell from SF analysis while NWW3 gives a SE swell direction.

ANA and TAK and 1:7 for REA) compared to MAT (1:2). Fig. 14 shows that the swell-related noise at ANA (locked around 50°) is perpendicular to the major axis of the Anaa atoll. The azimuth observed at REA (20–30°) also corresponds to the direction normal to the Reao atoll major axis. At TAK, although there is a gap in the data in 2002 September and the swell-related noise is weak (TAK seems to be protected from the SW incoming swell), the observed noise azimuth also seems to be correlated with the atoll anisometric elongation. Interestingly, unlike Reao and Anaa, the Takaroa atoll is elongated along the NE-SW direction. The azimuth of its long axis is about 60°. The swell-related ground vibration during the austral winter is oriented at 330° for SW incoming swells and in the range 310°–330° during boreal winter, when swells arrived from the NW. In both cases, these swell-related azimuths are very close to the normal of the atoll major axis.

Wave refraction is the most likely physical process that may explain such control of the SF noise azimuth by the shape of the islands. Swells arriving at a large angle from the atoll elongation axis are progressively rotated by refraction as the water becomes shallow and the wave fronts arrive at the atoll parallel to the shore. The energy is at the same time progressively transmitted to the basement. By such progressive swell rotation, the dominant energy imparted by the swell to the atoll is hence expected to be generally normal to the shore and, therefore, the dominant ground vibration will be along the direction normal to the atoll's long axis.

Conversely, the more circular shape of Mataiva atoll (aspect ratio of 1:2) can explain why the azimuth of the ground vibration is much better correlated to the swell azimuth. In both seasons, the atoll response is parallel to the swell excitation direction (Fig. 14b). This can be explained by the fact that swell refraction around a circular atoll is expected to have a simple symmetry and the swell maximum energy is expected to occur along the swell incoming azimuth.

In summary, if most of the atoll seismic stations appear to be suitable to derive the swell amplitude from the microseismic noise analysis, the circularity of the atoll seems to be an important criterion in selecting a site to perform reliable seismic measurements of both the amplitude and the azimuth of the swell-related signal. Station MAT is, therefore, the best-suited atoll station for this purpose.

5.3 Swell azimuth estimation over the whole year 2003 from PPTL

We show Fig. 15 that the swell azimuths measured at the permanent PPTL station mostly fall into two categories, depending on the season and on the swell conditions. The NNW swells occur primarily during the period December to March, while the SSW swells dominate during the remaining of the year (i.e. from April to November). The azimuths estimated from seismic data generally fit the NOAA model prediction well, and follow the same trends of evolution. It seems, however, that the observed azimuth differs by 10–20 degrees from that of the NOAA model. For instance, all the large SSW swells occurring in April–May–June are measured to arrive from azimuths around 220–230°, while the NOAA model predicts azimuths of 200–210°. Such a systematic discrepancy could be related to a structural effect of Tahiti island, but more likely to wave refraction along the coasts.

In 2003 February, we observe a swell event with a clear signature in the time series of both the predicted and the observed azimuths, but with a systematic difference of 70 degrees between them. The NOAA model predicted an approximately SE mean direction, while we observed a broadly SW incoming direction. This difference is likely related to the fact that the NOAA dominant wave height probably corresponds to short period swell (triangles on Fig. 15), while the swell values derived from seismic noise measurements are restricted to the long period ($Tp > 13$ s) swells (squares). This is visible on this diagram: the largest discrepancies between the observed microseismic noise azimuth and the predicted swell azimuth correspond systematically to swells of peak period Tp lower than 13 s (triangles).

6 QUANTIFICATION OF SWELL AMPLITUDE FROM INFRASONIC NOISE

In this section, we take advantage of an infrasonic mini-array installed in Tahiti island in order to provide an independent way to quantify the swell activity in the southern Pacific ocean. By combining two independent geophysical observables, the seismic (ground displacement) and the infrasonic (air pressure variations) signals recorded on Tahiti island, we show that the respective 'noise' amplitudes display very similar variations in the SF band that strongly suggest a common origin: the first corresponding to elastic waves propagating through the Earth and the second to infrasonic atmospheric waves, both being generated by the ocean swell-related oscillations.

6.1 Infrasonic noise measurement on Tahiti island

An infrasonic mini-array (code name I24FR) of 5 stations is in operation in Tahiti in the framework of the CTBT (Comprehensive Test Ban Treaty)-Organization (see Fig. 16 for the location and Le Pichon *et al.* (2002) for the description of the network). These stations, which provide a real-time, continuous record, comprise microbarometers whose data are digitized at a sampling rate of 20 Hz, with a sensitivity range of 1 mPa to 100 hPa and a flat instrumental response from 5 Hz to 10 mHz.

The infrasonic background noise has its origin in two principal types of natural phenomenon: the wind and the oceanic swell. Of these, the wind is the primary cause of noise, producing very large perturbations approximately equally over the entire spectrum from

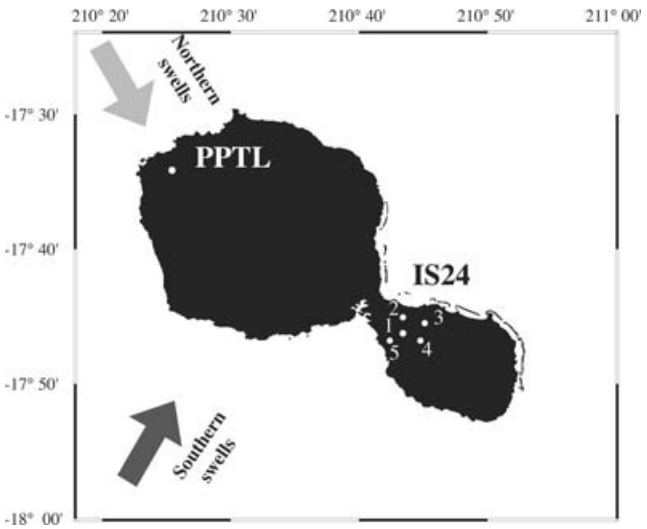

Figure 16. Map of Tahiti island showing the location of PPTL seismic station together with the I24FR infrasound array. The numbers 1 to 5 locate the infrasonic stations TAB1 to TAB5, respectively. Arrows indicate the directions of the dominant swell during the boreal winter (in grey) and the austral winter (in black).

long period to high frequency oscillations. Since the noise covers the entire useful bandwidth of the infrasonic signal, it is not practical to remove it by filtering. The most efficient way to reduce the wind-related noise is to use sites in forests, where the dense vegetation may locally reduce the wind speed. A second way, which we employed for the Tahiti network, is to perform a spatial filtering by the use of several tens of air vents, which are summed together. This analog summation of incoherent noise increases the signal-to-noise ratio. Fortunately, the wind in this tropical island location blows mainly during the daytime (e.g. Laurent *et al.* 2004) and is much weaker at night. Thus the microbarometers can record good quality data for at least half of the day.

A typical infrasound spectrum is presented Fig. 17. In general, the noise level increases toward low frequencies. A 'double frequency' peak around 0.2 Hz is clearly visible, as in Le Pichon *et al.* (2004). These authors suggest that this peak could be induced by distant standing waves related to low-pressure systems. The peak frequency is, therefore, controlled by the dominant wave frequency in the source area. By analysing infrasonic data recorded in Netherlands, Evers & Haak (2001) interpret their DF peak as the effect of oscillatory standing oceanic waves occurring in the north Atlantic. The SF, 'primary peak', centred around 0.06 Hz in the spectra in Fig. 17 is often masked by low frequency noise. The SF peak appears only during periods of low noise levels and high swell, which, therefore, suggests a local, swell-related origin. The use of infrasonic data to quantify swell is hence restricted to low wind periods. It should be noted that one cannot expect the DF peak to be exactly twice the SF frequency, as they have independent origins.

6.2 Seismic and infrasonic swell-related noise analysis on Tahiti

In 2003 April, a period of simultaneous low wind and high swell provides the opportunity to analyse together the infrasonic and the seismic noise amplitude variations on Tahiti island. We show below that the high-frequency 'surf noise' in the infrasound data is produced by swell breaking on the reef. We also show that the correlation between the infrasonic and the seismic noise amplitude in the SF range (0.05–0.077 Hz) is evidence that swell also provides an important source of infrasonic noise in this bandwidth.

The infrasound signal is processed with the progressive multi channel correlation (PMCC) method (Cansi 1995). This method enables infrasound events to be detected automatically. Each event is characterized by its azimuth and apparent velocity in several frequency bands: High frequencies (1–4 Hz), low frequencies (0.02–0.1 Hz) and long period gravity waves (1–5 mHz).

At high frequency, most of the detected events have a 'surf noise' origin, that is, they are generated by the oceanic swell breaking on the reef shore (Garcés *et al.* 2002), each breaking wave producing a single local signal, well detected by the infrasonic array, (Le Pichon *et al.* 2004). By identifying the arrival times of a given event at each infrasonic station, one is able to obtain a precise value of the source direction. Such PMCC-derived azimuths do not represent the swell azimuth itself, but instead the direction of the source of surf noise relative to the infrasonic station. Le Pichon *et al.* (2004) clearly demonstrate that the high frequency sources recorded in Tahiti occur along the barrier reef close to the infrasonic stations TAB4 and TAB5. The high frequency noise recorded at the infrasonic array can, therefore, be used to discriminate between the northward and southward swell propagation: between November and March, most of the surf noise is indeed located on the northern side of the network whereas between March and October, most of the surf noise is located on the southern reef.

An example of the variations of the infrasound amplitudes (in Pa) at longer periods (0.05–0.077 Hz) recorded at two different stations TAB4 and TAB5 is shown in Fig. 18 (a) for a selected period of low wind (2003 April 10 to 2003 May 5). Also plotted in Fig. 18 (a) are the NOAA predicted swell amplitudes for Tahiti. The variation of the microseismic SF 'noise' amplitude (0.05 to 0.077 Hz), recorded at station PPTL (see location in Fig. 16), is also plotted in Fig. 18 (b) for the same period, together with the same NOAA-predicted swell height variation. The obvious correlation between the infrasonic and the corresponding microseismic noise amplitude variations suggest a common origin. One possibility is that the microbarometers, like the seismometers, are responding to the ground movement. If this is the case, either the microbarometers could react as seismometers to the ground acceleration itself or they could record the air displacement produced by the ground displacement. Before discussing the relation between the variation of the air pressure and the swell, we test and quantify these two hypotheses. For this purpose, we analyse the record of a large seismic event (Loyalty Islands, 2004 January 3, Magnitude 7.1, latitude: 22.35°S, longitude: 169.61°E, depth: 10 km) which gives a clear signal at both the Tahiti PPTL seismic station and at the infrasonic network (having a duration of about 15 min on this network).

The Rayleigh waves generated by this Loyalty event induced a zero-to-peak ground motion of 230 μm at PPTL. By a double derivation of the signal, we deduce that it produced a maximum acceleration of about 30 μm s^{-2}. Since the microbarometer has a 0.81 V m^{-1} s^{-2} and a 20 mV/Pa sensibility, the ground acceleration of 3×10^{-5} m s^{-2} should produce a 'virtual' pressure signal of 1.22 10^{-3} Pa, which is about 25 times lower than the observed infrasonic signal, which is in the range 0.03–0.04 Pa, depending on the station. This simple calculation proves that the 'virtual' pressure signal generated by the ground acceleration produced by the Loyalty seismic event is much lower than the background noise level.

The second hypothesis to be tested is that the vertical ground displacement induces an air pressure fluctuation. Such a ground vibration should create a pressure variation given by:

$$P(\omega) = \rho c V(\omega).$$

Since the ground velocity for the Loyalty event derived from the PPTL seismogram is approximately 70×10^{-6} m s^{-1} and, taking the value of ρ to be 1.3 kg m^{-3} and the value of c to be 350 m s^{-1}, we obtain a value of 3.4×10^{-2} Pa for the pressure variation induced by the air fluctuation related to the vertical displacement generated by the Rayleigh wave. This value agrees very well with that which is observed at the individual infrasonic stations for this large earthquake. Our calculation, therefore, demonstrates that the infrasonic signal recorded during a strong seismic event is clearly associated with the air pressure fluctuation related directly to the ground motion.

We now consider the implications of the above result with regard to the swell-related ground vibration. If the 200 μm of vertical ground displacement of Tahiti island caused by the Rayleigh waves generated by a strong seismic event induced an infrasonic signal of 3.4×10^{-2} Pa, it is clear that the 1 μm of the swell-related ground vibration shown in Fig. 18(b) cannot explain a pressure signal of 2×10^{-2} Pa recorded simultaneously at the infrasonic stations. The pressure variation measured in the 0.05–0.077 Hz frequency range by the infrasonic stations is, therefore, a true atmospheric signal, likely to have been produced by the swell-related air oscillation above the neighbouring ocean. Thus we have shown that the clear

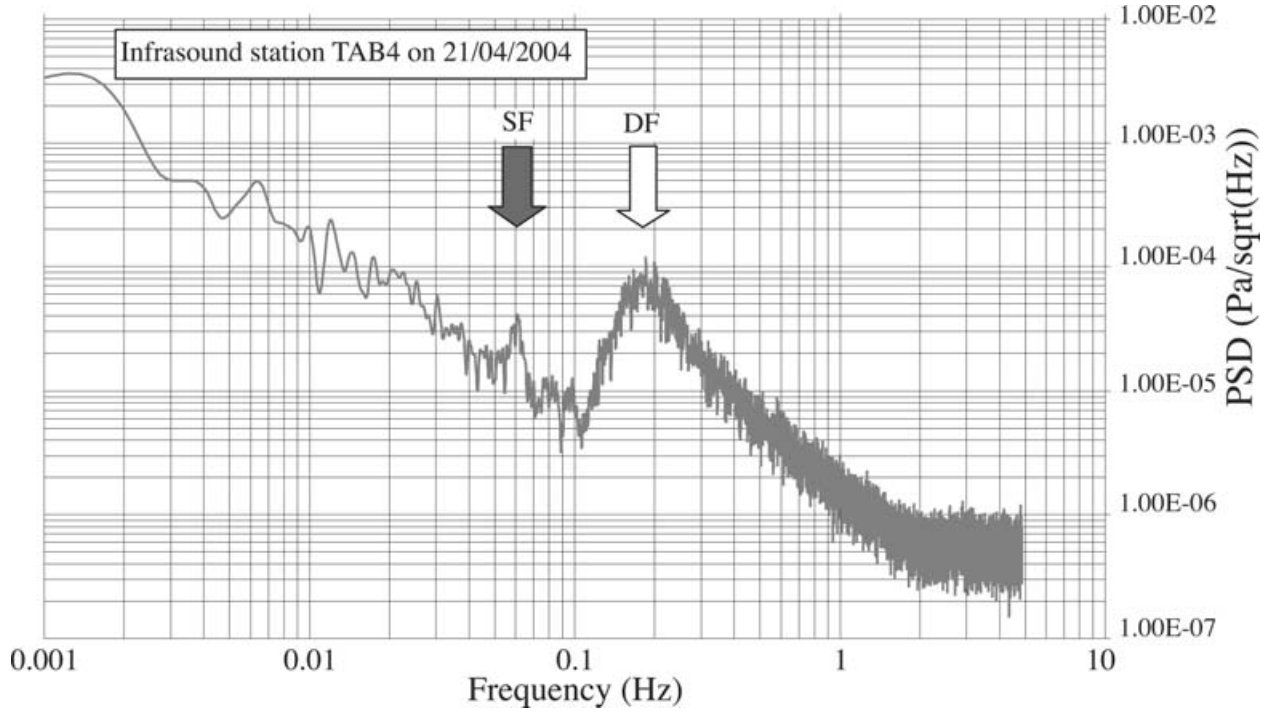

Figure 17. Example of infrasound spectrum obtained at station TAB4 on 2003 April 21. During this period of weak winds and strong swell, the spectra has a clear swell-related energy peak at about 0.06 Hz (indicated by 'SF'). The double frequency peak 'DF' is at about 0.2 Hz.

correlation between the infrasonic and seismic 'noise' amplitudes (Figs 18a and b, respectively) can be explained if there is a common driving mechanism (swell), which produces independent signals in the atmosphere and ground. Both data sets were acquired on the same island, at about 50 km from each other, and are affected by the same phenomenon, the swell activity, which generates simultaneously elastic waves in the ground and infrasonic waves in the atmosphere. The correlation between the amplitude of the infrasonic signal and the amplitude of the swell demonstrates that infrasound can be an independent quantifier of swell activity.

The best fit between the predicted significant height of the swell calculated by the NOAA 'WaveWatch' model and infrasound amplitude is found to be a log relationship as follows:

$$Hs = 2.48\ \ln(P) + 12.6,$$

where *Hs* is the predicted swell height in *m* and *P* is the pressure in *Pa* measured at the closest station from the shore (TA4).

The correlation coefficient *R* has a value of 0.81. This confirms that infrasonic analyses provide a complementary and independent approach to quantify the swell height, with the restriction that measurements should be made during low wind periods.

The PMCC analysis of this signal did not provide a coherent result regarding azimuths, which means that it is not possible accurately to determine the location of the infrasonic source. This may be explained by the fact that the whole neighbouring ocean may act as a source.

7 CONCLUSIONS

By analysing the spectral content of data from seismic stations installed in French Polynesia in the South Pacific, we show that ocean swell generates a clear peak in the 'single frequency' band of the microseismic noise, that is, for periods ranging from 13 to 20 s. The spectral analysis also provides evidence that the swell-related microseismic noise is primarily contained within the horizontal plane and corresponds to an elliptical ground motion.

The quantification of the microseismic noise in this (0.05–0.077 Hz) frequency range is achieved by the measurement of the ground particle motion. The length and the azimuth of the elliptical ground motion respectively give the amplitude and the azimuth of the noise. We show that the amplitude of this microseismic noise is highly correlated with the swell height at most seismic stations and, therefore, provides a way to monitor swell activity from a seismic record. For the noise azimuth, the best correlation with the swell direction is observed on islands with a small elongation ratio. For the stations in the Tuamotu archipelago installed on elongated atolls, we observe that the atoll generally has a preferred direction of vibration, normal to its long axis, suggesting a strong influence of wave refraction processes. We conclude that a seismic station installed on a roughly circular island is best suited to quantify simultaneously the swell height and azimuth with good accuracy.

The infrasound network installed in Tahiti provides an independent and complementary technique to quantify the swell height. We show that the infrasonic noise in the SF frequency range is correlated with both the swell height and the swell-related microseismic noise recorded at the station PPTL installed on Tahiti.

We finally demonstrate that the PPTL permanent seismic station installed in Tahiti is suitable to monitor the swell activity in real time. Moreover, its long-term recording capability provides a way to analyse long-term swell variations that could be related to climate changes.

ACKNOWLEDGMENTS

PLUME is financed by the French Ministère de la Recherche, Action Concertée Incitative (ACI) jeunes chercheurs, and supported by the Commissariat à l'Energie Atomique (CEA). Many thanks to

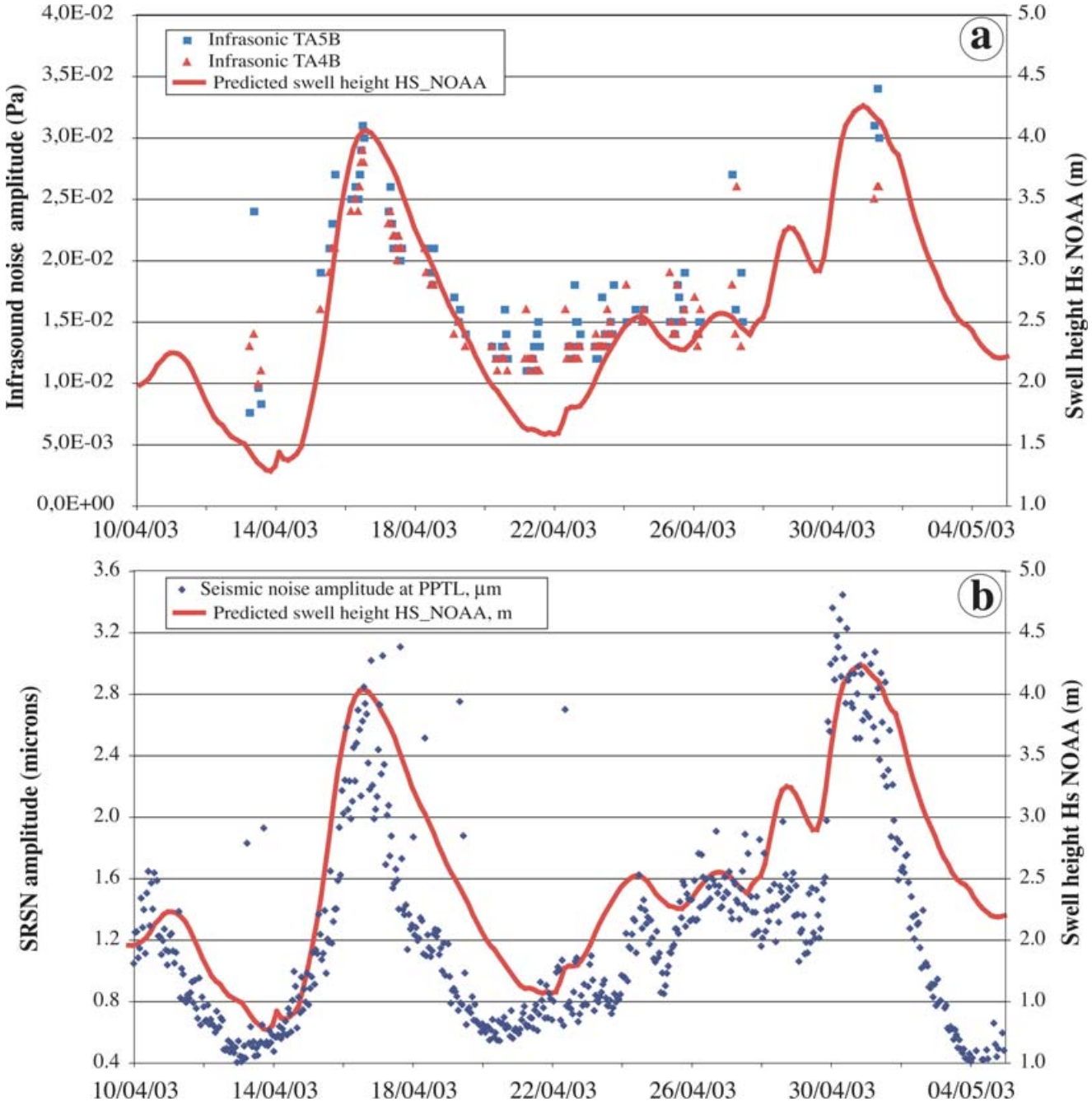

Figure 18. (a) Variation of the measured amplitude (in Pa) of the infrasound during the period 2003 April 12 to May 2, at two sites, TA4B and TA5B, together with the variations of the NOAA-predicted swell height *Hs* (red line, in m). This period was particularly suited to test the possible correlations between swell height, infrasonic and seismic noise because of the absence of wind and the presence of a high swell. (b) Variation of the microseismic noise amplitude (blue dots, in microns) at station PPTL in the 0.05–0.077 Hz range, together with the NOAA predicted swell height *Hs*. The correlation of both the infrasonic and seismic noise with the swell amplitude suggests that both signals have a common source and that both are potential proxies for the swell height.

the Centre National de la Recherche Scientifique (CNRS), to the Government of French Polynesia and the Université de Polynésie française (UPF) for having made possible this experiment. Portable seismic stations were kindly provided by the Institut National des Sciences de l'Univers (INSU), the Réseau Large Bande Mobile (RLBM) efficiently managed by J.J. Lévèque and J. Burdin (EOPG Strasbourg). We are extremely thankful to Météo France and to the Aviation Civile for having made possible the installation of seismic stations on their sites and for the useful and efficient help provided by their personnel and by the municipalities of the islands. Thanks to Victoire Laurent of Météo France for providing us with synoptic swell measurements around Tahiti. Many thanks to Hilary Todd for the helpful final reading of the manuscript and to two anonymous reviewers who carefully read and commented on the manuscript.

REFERENCES

Aki, K. & Richards, P.G., 1980. *Quantitative seismology. Theory and Methods*, pp. 557, W.H. Freeman and Co., New York.

Barruol, G. et al, 2002. PLUME investigates South Pacific Superswell, *EOS, Trans. Am. geophys. Un.,* **83,** 511–514.

Barruol, G., Legendre, C., Masson, F., Vergne, J., Fontaine, F. & Bokelmann, G.H.R., 2004. The transition zone beneath the south Pacific superswell from receiver function analyses, *EOS, Trans. Am. geophys. Un.,* **85,** (47), Fall Meeting Suppl., Abstract T41G-06.

Barstow, N., Sutton, G.H. & Carter, J.A., 1989. Particle motion and pressure relationships of ocean bottom noise: 3900 m depth; 0.003 to 5 Hz, *Geophys. Res. Lett.,* **16,** 1185–1188.

Beauduin, R. & Montagner, J.P., 1996. Time evolution of broadband seicmic noise during the french pilot experiment OFM/SISMOBS, *Geophys. Res. Lett.,* **23**(21), 2995–2998.

Bonneville, A. & Sichoix, L., 1998. Topographie des fonds océaniques de la Polynésie française: synthèse et analyse, *Géologie de la France,* **3,** 15–28.

Booij, N. & Holthuijsen, L.H., 1987. Propagation of ocean waves in discrete spectral wave models, *J. Comput. Phys.,* **68,** 307–326.

Booij, N., Ris, R.C. & Holthuijsen, L.H., 1999. A third-generation wave model for the coastal regions, Part I, Model description and validation, *J. geophys. Res.,* **104,** 7649–7666.

Bromirski, P.D., 2001. Vibrations from the 'Perfect Storm', *Geochem. Geophys. Geosyst.,* **2,** Paper number 2000GC000119.

Bromirski, P.D. & Duennebier, F.K., 2002. The near-coastal microseism spectrum: spatial and temporal wave climate relationships, *J. geophys. Res.,* **107**(B8), doi:10.1029/2001JB000265.

Bromirski, P.D., Flick, R.E. & Graham, N., 1999. Ocean wave height determined from inland seismometer data: implications for investigating wave climate changes in the NE Pacific, *J. geophys. Res.,* **104**(C9), 20 753–20 766.

Cansi, Y., 1995. An automatic seismic event processing for detection and location: The P.M.C.C. method, *Geophys. Res. Lett.,* **22**(9), 1021–1024.

Cessaro, R.K., 1994. Sources of primary and secondary microseisms, *Bull. seism. Soc. Am.,* **84**(1), 142–148.

Chave, A., Thompson, D.J. & Ander, M.E., 1987. On the robust estimation of power spectra, coherences, and transfert functions, *J. geophys. Res.,* **92,** 633–648.

Clouard, V. & Bonneville, A., 2004. Submarine landslides in French Polynesia, in *Oceanic hot spots*, pp. 209–238, eds Hekinian, R., Stoffers, P. & Cheminée, J.L., Springer Verlag.

Darbyshire, J. & Okeke, E.O., 1969. A study of primary and secondary microseisms recorded in Anglesey, *Geophys. J. R. astr. Soc.,* **17,** 63–92.

Evers, L.G. & Haak, H.W., 2001. Listening to sounds from an exploding meteor and oceanic waves, *Geophys. Res. Lett.,* **28**(1), 41–44.

Fontaine, F., Barruol, G., Reymond, D., Debayle, E. & Tommasi, A., 2002. Seismic Anisotropy of the French Polynesian Upper Mantle: PLUME Preliminary Results, *EOS, Trans. Am. geophys. Un.,* **83,** (47), Fall Meeting Suppl., Abstract S11A-1127.

Garcés, M., Hezter, C., Businger, S. & Willis, M., 2002, 24th Seismic Research Review—Nuclear Explosion Monitoring: Innovation and Integration, pp. 766–774, Ponte Vedra, Florida.

Grevemeyer, I., Herber, R. & Essen, H.H., 2000. Microseismological evidence for a changing wave climate in the northeast Atlantic Ocean, *Nature,* **408,** 349–352.

Hasselmann, K., 1963. A statistical analysis of the generation of microseisms, *Rev. Geophys.,* **1,** 177–210.

Haubrich, R.A. & McCamy, K., 1969. Microseisms: Coastal and pelagic sources, *Rev. Geophys.,* **7,** 539–571.

Hedlin, M.A.H. & Orcutt, J.A., 1989. A comparative study of island, seafloor, and subseafloor ambient noise levels, *Bull. seism. Soc. Am.,* **79,** 172–179.

Hoteling, H., 1933. Analysis of a complex of statistical variables into principal components, *J. Educ. Psychology,* **24,** 417–441.

Hyvernaud, O., Reymond, D., Talandier, J. & Okal, E., 1993. Four years of automated measurements of seismic moments at Papeete using the mantle magnitude Mm; 1987 1991., *Tectonophysics,* **217,** 175–193.

Jordahl, K.A., Caress, D.W., McNutt, M.K. & Bonneville, A., 2004. Seafloor morphology of the South Pacific Superswell region, in *Oceanic Hot Spots*, pp. 9–28, eds Hekinian, R., Stoffers, P. & Cheminée, J.L., Springer Verlag, New York.

Kanamori, H., 1989. A slow event recorded in Pasadena, *Geophys. Res. Lett.,* **16**(12), 1411–1414.

Kibblewhite, A.C. & Ewans, K.C., 1985. Wave-wave interactions, microseisms, and infrasonic ambient noise in the ocean, *J. acoust. Soc. Am.,* **78,** 981–994.

Laurent, V., Maamaatuaiahutapu, K., Maiau, J. & Varney, P., 2004. *Atlas climatologique de la Polynésie française*, 201 pp. Météo France—Direction Interregionale de Polynésie Française, Papeete.

Le Pichon, A., Guérin, J.M., Blanc, E. & Reymond, D., 2002. Trail in the atmosphere of the 29 december 2000 meteor as recorded in Tahiti: characteristics and trajectory reconstruction, *J. geophys. Res.,* **107**(D23), doi:10.1029/2001JD001283.

Le Pichon, A., Maurer, V., Reymond, D. & Hyvernaud, O., 2004. Infrasound from ocean waves observed in Tahiti, *Geophys. Res. Lett.,* **31,** (L19103), doi:10.1029/2004GL020676.

Longuet-Higgins, M.S., 1950. A theory of the origin of the microseisms, *Phil. Trans. Roy. Soc.,* **243,** 1–35.

Maggi, A., Debayle, E., Priestley, K., Barruol, G., Fontaine, F. & Reymond, D., 2003. The upper mantle under the south pacific super-swell from multimode surface waveform tomography, *EOS, Trans. Am. geophys. Un.,* **84,** (46), Fall Meeting Suppl., Abstract V21F-03.

Müller, T. & Zürn, W., 1983. Observation of gravity changes during the passage of cold front, *J. geophys. Res.,* **53,** 155–162.

Pearson, K., 1901. On lines and planes of closest fit to system of points in space, *Phil. Mag.,* **2**(11), 559–572.

Peterson, J., 1993. Observation and modeling of seismic background noise, *US Geol. Surv. Open File Rep,* **93–322,** 1–95.

Rancher, J. & Rougerie, F., 1995. L'environnement océanique de l'archipel des Tuamotu (Polynésie française), *Océanologica Acta,* **18**(1), 43–59.

Rasolofosaon, P.N., Zinszner, B. & Johnson, P.A., 1997. Propagation des ondes élastiques dans les matériaux non linéaires, *revue de l'institut français du pétrole,* **52**(6), 585–608.

Reymond, D., Hyvernaud, O. & Talandier, J., 1991. Automatic detection, location and quantification of earthquakes; application to tsunami warning, *Pure appl. Geophys.,* **135,** 361–382.

Schulte-Pelkum, V., Earle, P.S. & Vernon, F., 2004. Strong directivity of ocean-generated seismic noise, *Geochem. Geophys. Geosyst.,* **5**(3), doi:10.1029/2003GC000520.

Shapiro, N.M., Campillo, M., Stehly, L. & Ritzwoller, M.H., 2005. High-resolution surface-wave tomography from ambient seismic noise, *Science,* **307,** 1615–1618.

Sorrels, G.G., 1971. A preliminary investigation into the relationship between long-period seismic noise and local fluctuations in the atmospheric pressure field, *Geophys. J. R. astr. Soc.,* **26,** 71–82.

Sorrels, G.G., McDonald, J.A., Der, Z.A. & Herrin, E., 1971. Earth motion caused by local atmospheric pressure changes, *Geophys. J. R. astr. Soc.,* **26,** 83–98.

Stutzmann, E., Roult, G. & Astiz, L., 2000. GEOSCOPE station noise levels, *Bull. seism. Soc. Am.,* **90,** 690–701.

Talandier, J. & Hyvernaud, O., 1991. Les mesures de houles bruit de fond microsismique, *Ocean, Space Advanced Technologies European Show*, IFREMER, Brest, France.

Talandier, J. & Okal, E., 1987. Crustal structure in the Society and Tuamotu islands, French Polynesia, *Geophys. J. R. astr. Soc.,* **88,** 499–528.

Talandier, J., Hyvernaud, O., Okal, E. & Piserchia, P.F., 2002. Long-range detection of hydroacoustic signals from large icebergs in the Ross sea, Antarctica, *Earth planet. Sci. Lett.,* **203,** 519–534.

Tolman, H.L., 2001. Improving propagation in ocean wave models, in *Ocean Wave Measurements and Analysis*, pp. 507–516, eds Edge, B.L. & Hemsley, J.M., San Francisco, California.

Tolman, H.L. & Chalikov, D.V., 1996. Source terms in a third-generation wind wave model, *J. Phys. Oceanogr.,* **26,** 2497–2518.

Webb, S.C., 1998. Broadband seismology and noise under the ocean, *Rev. Geophys.,* **36,** 105–142.

Zürn, W. & Widmer, R., 1995. On noise reduction in vertical seismic records below 2mHz using local barometric pressure, *Geophys. Res. Lett.,* **22**(24), 3537–3540.